ARTICLE

C, O, and Sr isotopic variations in Neoproterozoic-Cambrian carbonate rocks from Sete Lagoas Formation (Bambuí Group), in the Southern São Francisco Basin, Brazil

Variações isotópicas de C, O e Sr em rochas carbonáticas do Neoproterozoico-Cambriano da Formação Sete Lagoas (Grupo Bambuí), no Sul da Bacia do São Francisco, Brasil

**Cristian Guacaneme[1], Marly Babinski[1]*,
Gustavo Macedo de Paula-Santos[1], Antonio Carlos Pedrosa-Soares[2]**

ABSTRACT: High-resolution chemostratigraphic data of carbonates from the Sete Lagoas Formation (Bambuí Group) show large variations on the C, O, and Sr isotope compositions. Impure limestones at the base show primal $\delta^{13}C$ values between -1.0 and 0‰, and $\delta^{18}O$ values between -12.0 and -8.0‰. However, some dolostones demonstrate $\delta^{13}C$ values varying from +2.8 to -6.8‰, highly radiogenic $^{87}Sr/^{86}Sr$ ratios (>0.7111), and low Sr concentrations (<350 ppm) related to post-depositional processes. In contrast, pure limestones at the top show very positive $\delta^{13}C$ values between +8.3 and +12.8‰, $\delta^{18}O$ values between -10.0 to -6.0‰, and $^{87}Sr/^{86}Sr$ ratios from 0.7073 to 0.7086, with high Sr concentrations (>900 ppm). They are linked to depositional controls on the carbonate platform, such as fluvial and/or submarine water influx, in which carbonates deposited on the proximal sector exhibit significant Sr isotopic variations and those on the distal sector were not subject to such controls, resulting in very homogeneous Sr isotope profiles. However, $^{87}Sr/^{86}Sr$ ratios of the distal carbonates are less radiogenic than carbonates expected for late Ediacaran (~0.7085). This discrepancy suggests a restricted marine basin without Sr isotopic homogenization with contemporary oceans and, in this case, global correlations based on Sr isotope stratigraphy are not reliable.

KEYWORDS: Isotopes; Carbonates; Bambuí Group; Ediacaran.

RESUMO: *Dados quimioestratigráficos de alta resolução em carbonatos da Formação Sete Lagoas (Grupo Bambuí) apresentam grandes variações nas composições isotópicas de C, O e Sr. Os calcários impuros na base da unidade mostram valores primários de $\delta^{13}C$ entre -1,0 e 0‰ e de $\delta^{18}O$, entre -12,0 e -8,0‰. No entanto, alguns níveis de dolomitos indicam valores de $\delta^{13}C$ variando de +2,8 a -6,8‰ e razões $^{87}Sr/^{86}Sr$ altamente radiogênicas (>0,7111), além de baixas concentrações de Sr (<350 ppm) relacionadas a processos pós-deposicionais. Em contraste, os calcários puros no topo da unidade demonstram valores de $\delta^{13}C$ muito positivos entre +8,3 e +12,8‰, de $\delta^{18}O$ entre -10,0 e -6,0‰ e razões $^{87}Sr/^{86}Sr$ de 0,7073 a 0,7086, com altas concentrações de Sr (>900 ppm). Esses estão ligados a controles deposicionais na plataforma carbonática, tais como fluxos de água fluvial e/ou submarina, em que os carbonatos depositados no setor proximal exibem variações isotópicas de Sr significativas e os depositados no setor distal não estão sujeitos a tais controles, resultando em perfis isotópicos de Sr homogêneos. No entanto, as razões $^{87}Sr/^{86}Sr$ dos carbonatos distais são menos radiogênicas do que aquelas esperadas para o Ediacarano tardio (~0,7085). Essa discrepância sugere um ambiente deposicional em uma bacia marinha restrita, sem homogeneização isotópica de Sr com oceanos contemporâneos e, neste caso, as correlações globais baseadas na estratigrafia isotópica de Sr não são confiáveis.*

PALAVRAS-CHAVE: *Isótopos; Carbonatos; Grupo Bambuí; Ediacarano.*

INTRODUCTION

Neoproterozoic carbonate sequences overlying glacial deposits, also known as cap carbonates, have been widely used as regional and global chemostratigraphic correlation tools due to their characteristic negative carbon isotopic signature and lack of reliable biostratigraphy (Kennedy, 1996; Kaufman *et al.*, 1997; Hoffman *et al.*, 1998; Jacobsen & Kaufman, 1999; Hoffman & Schrag, 2002). During the Cryogenian, the Sturtian (~720 Ma) and Marinoan (~635 Ma) low-latitude global glaciations (Halverson *et al.*, 2005, Hoffman & Li, 2009) isolated the atmosphere of oceans, thus creating low bio-productivity of photosynthetic marine organisms, and also generated ^{12}C accumulation in the oceans, as proposed in the "Snowball Earth" hypothesis (Kirschvink, 1992; Hoffman *et al.*, 1998). After the retreat of glaciers and marine transgression by global warming, carbonates deposited immediately after glaciations recorded negative excursions in the $\delta^{13}C$ values. During the Ediacaran, the Gaskiers glaciation (~582 Ma) may have had a different scenario, with geochemical signals for a significant oxygenation event in deep sea and through the appearance of complex eukaryotes (Narbonne, 2008). Nevertheless, many researchers find the overall character of $\delta^{13}C$ values a challenge (Melezhik *et al.*, 2001; Eyles & Januszczak, 2004; Derry, 2010; Frimmel, 2010), since the carbon isotope anomalies may represent post-depositional processes, rather than global or restricted depositional environments.

The Sete Lagoas Formation overlies diamictites and glacial deposits in the East of central Brazil. It is identified as a cap carbonate of Sturtian age (Babinski *et al.*, 2007; Vieira *et al.*, 2007b). This unit shows strong negative $\delta^{13}C$ values of -5‰ at the base that increase to 0‰ in the intermediate part of the sequence, and abruptly change to very positive values as high as +16‰ at the top, accompanied by alterations on the sedimentary facies. This enables the subdivision of Sete Lagoas Formation into lower and upper sequences separated by a positive carbon isotopic shift (Vieira *et al.*, 2007b). However, some authors propose that the Sete Lagoas Formation represents a cap carbonate sequence of early Ediacaran age deposited after the Marinoan glaciation, based on global correlations via isotope chemostratigraphy (i.e. Caxito *et al.*, 2012; Alvarenga *et al.*, 2014; Uhlein *et al.*, 2016). To add more pieces to the puzzle, recent biostratigraphic data indicate ages of 553-542 Ma in the middle part of the sequence based on *Cloudina* fossil (Warren *et al.*, 2014), which suggest a late Ediacaran age for the Sete Lagoas Formation. This is consistent with the U-Pb age of 560 Ma obtained from detrital zircon grains of the upper sequence, interpreted as the maximum depositional age (Paula-Santos *et al.*, 2015).

The $^{87}Sr/^{86}Sr$ ratios between 0.7074 and 0.7080 indicate ambiguity in the age of the Bambuí Group (Misi *et al.*, 2007;

Babinski *et al.*, 2007; Kuchenbecker, 2011; Alvarenga *et al.*, 2014; Paula-Santos *et al.*, 2015) in comparison with the seawater Sr isotope evolution curves proposed in literature (Jacobsen & Kaufman, 1999; Melezhik *et al.*, 2001; Halverson *et al.*, 2010; Kuznetsov *et al.*, 2013). Considering the maximum depositional age of 560 Ma, such Sr isotope ratios are lower than the ones expected for the terminal Ediacaran. Paula-Santos *et al.* (2015) interpreted that the orogenic belts surrounding the São Francisco craton created a restricted marine environment during the late Neoproterozoic, thus preventing isotope homogenization between the São Francisco basin and the global pool. The complexity of the geological context and the difficulty to position stratigraphically the Bambuí Group justify a detailed geochemical and isotopic study on the carbonate platform together with the sedimentary characteristics, in an attempt to elucidate the current discussions in view of a restricted depositional environment.

GEOLOGICAL CONTEXT AND STUDY AREA

The São Francisco Basin

The São Francisco Basin extends for much of Eastern Brazil, approximately 300.000 km² exposed in Minas Gerais, Bahia, and Goiás states (Almeida, 1977). The basin basement consists of Archean and Paleoproterozoic granitoids (Alkmim & Marshak, 1998; Teixeira *et al.*, 2000) named the São Francisco Craton, which are bounded by Neoproterozoic orogenic belts of the Pan-African/Brasiliano orogeny (Chemale *et al.*, 1993; Alkmim *et al.*, 1996; Teixeira *et al.*, 2000) known as Brasília Belt in the West, Araçuaí Belt in the East, and Rio Preto, Riacho do Pontal and Sergipano orogenic belts in the Northern limits of the craton (Fig. 1). These Neoproterozoic orogenic belts have thrust faults and folds with differentiated tectonic features in their lateral limits (Alkmim *et al.*, 1996; Alkmim and Martins-Neto, 2001; Coelho *et al.*, 2008). The African counterpart of the São Francisco Craton is the Congo Craton, which extends over a wide area in the Western part of Central Africa. The basement consists of a large Archean-Paleoproterozoic core bounded by the Oubanguides, Kibaran, Damara, and West Congolian orogenic belts (Alkmim & Martins-Neto, 2012). Alkmim & Martins-Neto suggest that the São Francisco-Congo continent and various fragment derivatives of Rodinia began to converge at the end of the Cryogenian period, and the reassembly resulted in the formation of the Gondwana supercontinent in the Ediacaran. In such process, the edges of the São Francisco-Congo continent were diachronically converted into mobile belts for the Pan-African/Brasiliano orogenic event, with an impact inside of the craton, which

behaved as a foreland basin, namely São Francisco basin. The basic stratigraphy of the São Francisco basin comprises clastic deposits of Jequitaí and Carrancas formations at the base and carbonate-siliciclastic sediments of Bambuí Group at the top (Almeida *et al.*, 1976).

The basal Jequitaí Formation (~150 m thickness) contains diamictites, massive sandstones, and fine rhythmites deposited in marine and continental glacial environments (Dardenne, 1978; Rocha-Campos *et al.*, 1981). In the Southern region of the São Francisco Craton occurs the Carrancas Formation, which consists of diamictites with siltstone lenses directly overlying the basement and outcropping in local areas (Costa & Branco, 1961; Vieira *et al.*, 2007; Tuller *et al.*, 2009). This unit has glacial origin and correlates with diamictites of the Jequitaí Formation and Macaúbas Group (Martins-Neto *et al.*, 2001; Alkmim & Martins-Neto, 2001, 2012), and glacial deposits on the West Congolian Group exposed in Africa (Babinski *et al.*, 2012). However, some authors argue that there is no direct evidence for glacial deposition of the

Carrancas Formation in the type area (Vieira *et al.*, 2007; Tuller *et al.*, 2009, Uhlein *et al.*, 2016). The U-Pb maximum depositional ages based on detrital zircon are 1.4 and 1.2 Ga for the Carrancas Formation (Rodrigues, 2008; Guacaneme, 2015) and 0.9 Ga for the Jequitaí Formation (Buschwaldt *et al.*, 1999).

The Bambuí Group

Costa and Branco (1961) proposed the original stratigraphy of the Bambuí Group, which Dardenne (1978) then modified and subdivided into six lithostratigraphic units from the base to the top:

- Jequitaí Formation formed by diamictites, sandstones, and fine rhythmites;
- Sete Lagoas Formation (500 m thickness maximum estimate based on Iglesias & Uhlein, 2009) represented by stromatolitic limestones and dolomites with pelites;
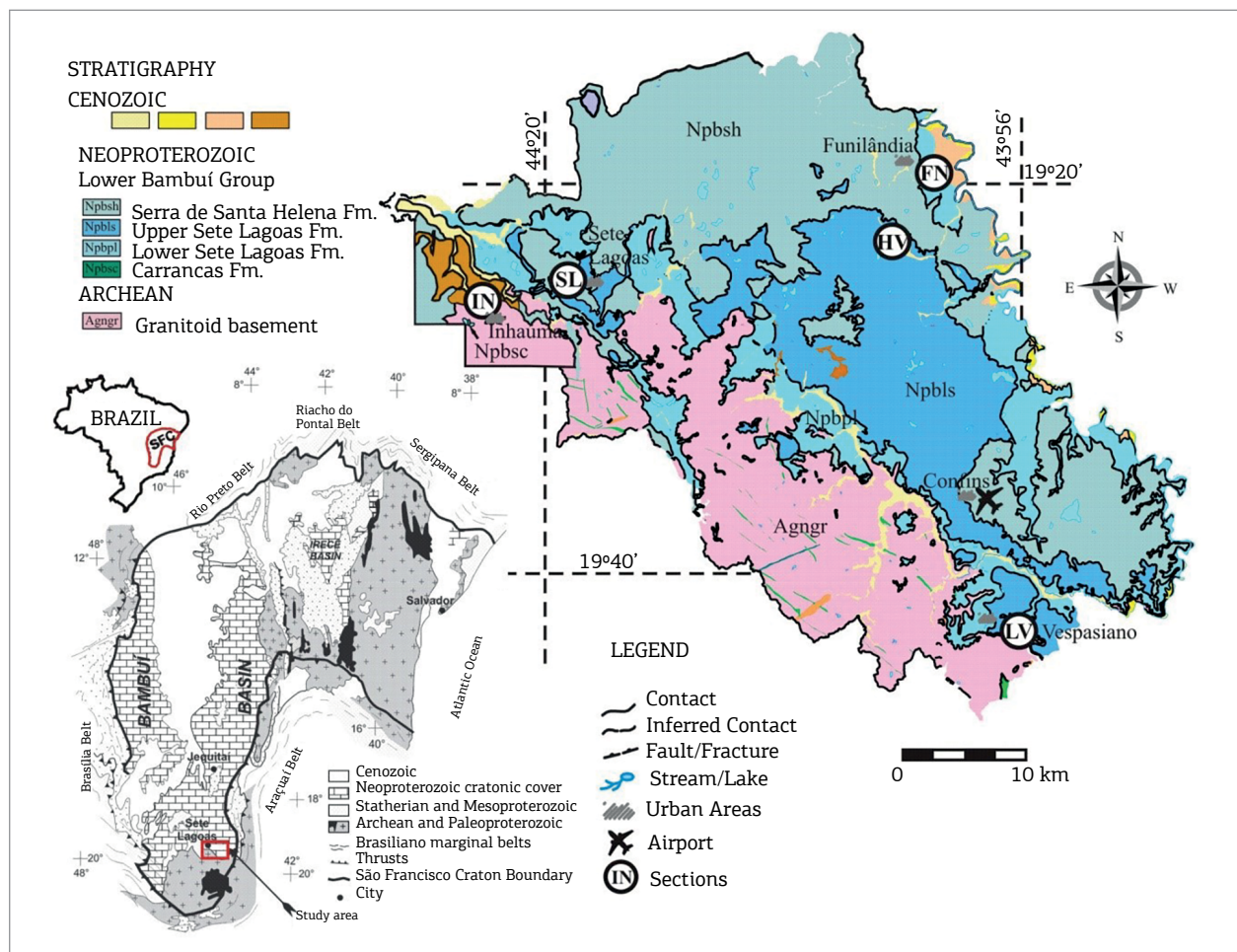- Serra de Santa Helena Formation (640 m) essentially pelitic with shales and siltstones;

Figure 1. Geological map of the São Francisco craton (Modified from Santos *et al.*, 2000) and study area with location of stratigraphic sections. Sete Lagoas (SL), Haras Veredas (HV), Linha Verde (LV), Inhaúma (IN) and Funilândia (FN) sections (Modified from Ribeiro *et al.*, 2003).

- Lagoa do Jacaré Formation (350 m) formed by oolitic and pisolitic limestones with siltstones and marl lens;
- Serra de Saudade Formation (200 m) consisting of shales, siltstones, and pelites; and
- Três Marias Formation consisting of siltstones and arkoses (Fig. 1).

The lower four units were deposited in a shallow marine environment, while the top unit was deposited in a shallow marine alluvial environment (Dardenne, 1978). The sedimentary sequence of Bambuí Group records a major transgression in a foreland marine basin generated in the overload caused by Neoproterozoic mobile belts, especially the thrust and crustal pressures of Brasília orogen along the West part of the São Francisco Craton (Alkmim & Martins-Neto, 2001, 2012; Martins-Neto *et al.*, 2001; Martins-Neto, 2005, 2009), as the product of arc-continent and continent-continent collision between 800 and 550 Ma (Pimentel *et al.*, 1999). Seismic data of this unit indicate thicknesses of about 4 km to the West and about 800 m to the East of the São Francisco Craton, near the flexural edge (Martins-Neto, 2005).

The Sete Lagoas Formation

The Sete Lagoas Formation consists of stromatolitic limestones, dolostones, and pelites covering diamictites and siltstones in the São Francisco Craton (Dardenne, 1978). Based on sedimentological and stratigraphic studies, Schöll (1976) subdivided the Sete Lagoas Formation into two main members: lower Pedro Leopoldo Member and upper Lagoa Santa Member (Fig. 1). The first (~100 m thick) consists of grey impure limestones, dolostones, and marls subordinated strata, with some deformed and recrystallized carbonate rocks. The Lagoa Santa Member (~150 m thick) consists of well preserved black pure limestones, lime mudstone, and siltstone subordinates. In the Southern part of the São Francisco Craton, Vieira *et al.* (2007a) recognized two megacycles for the Sete Lagoas Formation that record transgression events separated by an unconformable contact. These megacycles closely resemble the upper and lower members proposed by Schöll (1976). The first megacycle began with seafloor precipitates (aragonite pseudomorphs) and negative $\delta^{13}C$ values in the range of -5‰, which increased close to 0‰, with gradual disappearance of these precipitates (Fig. 1), leading to a transgression on the São Francisco Craton and depositing carbonates directly on the Archean-Paleoproterozoic basement. This megacycle ends with crystalline limestone and hummocky stratification, which indicate the influence of storm waves, and with $\delta^{13}C$ values oscillating in a narrow range close to 0‰. A broad deposition of limestones without wave structures marks the second megacycle, thus indicating deposition in a deep marine environment, below the level influence of waves and storms. These limestones are overlaid by carbonates with wavy and microbial structures deposited in coastal areas with very positive $\delta^{13}C$ values that reach +16‰ (Iyer *et al.*, 1995). This significant increase in the $\delta^{13}C$ values from the base to the top of the Sete Lagoas Formation was also reported by Santos *et al.* (2000, 2004), Misi *et al.* (2007), Alvarenga *et al.* (2014) and Paula-Santos *et al.* (2015).

The geochronological data presented for Sete Lagoas Formation is complex because different radiometric methods were used to obtain the Cryogenian and Ediacaran ages. Babinski *et al.* (2007) found a Pb-Pb isochron age of 740 ± 22 Ma in the basal cap carbonate rocks (Fig. 1), which positioned them as post-Sturtian in the global glaciations context. However, Rodrigues (2008) obtained a U-Pb detrital zircons age of 610 Ma in shales from the second megacycle proposed by Vieira *et al.* (2007a). Based on lithostratigraphic and isotopic data, Caxito *et al.* (2012) suggested that the Sete Lagoas Formation represents a cap carbonate sequence of lower Ediacaran age deposited after the Marinoan glaciation. To add more complexity, the discovery of the *Cloudina sp.* fossil in the Sete Lagoas Formation at the Januária region indicates an Ediacaran age of 553 – 542 Ma (Fig. 1). According to the paleogeographic position of the carbonate sequences with *Cloudina* in Brazil, Antarctica, Namibia, Argentina and Uruguay, an oceanic connectivity scenario of coeval intracratonic basins in the late Neoproterozoic can be suggested (Grotzinger *et al.*, 2000; Warren *et al.*, 2014). These latter authors obtained $\delta^{13}C$ values between 0.06 and 0.67‰ (V-PDV) in the fossiliferous carbonates, which place the *Cloudina* in the middle portion of the Sete Lagoas Formation, according to stratigraphic correlation with C isotopic data from Misi *et al.* (2007), Vieira *et al.* (2007b) and Paula-Santos *et al.* (2015).

In addition, Paula-Santos *et al.* (2015) reported U-Pb detrital zircon ages of 537 ± 4 Ma and 506 ± 6 Ma in pelitic sediments of the first and second sequences of the Sete Lagoas Formation, respectively, supported by U-Pb age of 560 Ma in the younger detrital zircon population (n = 16), which is interpreted as the maximum depositional age of the upper Sete Lagoas Formation. These data refute the possibility of unconformity between the lower and upper sequences of the Sete Lagoas Formation, with a deposition gap of approximately 200 m.y. If such gap exists, it is positioned between the basal cap carbonates with d^{13}C values as low as -5‰, and carbonates that preserve $\delta^{13}C$ values about 0‰ (Fig. 1). We note that an erosive unconformity surface compatible with such gap is yet to be recognized. The new U-Pb radiometric evidence from Paula-Santos *et al.* (2015) confirms an Ediacaran-Cambrian age of the Bambuí Group, but it does not imply necessarily that the base of the unit exhibits the same age. Therefore, the Cryogenian age of

740 Ma for the basal carbonates overlying glacial deposits proposed by Babinski *et al.* (2007) is still valid.

Low radiogenic $^{87}Sr/^{86}Sr$ ratios between 0.7074 and 0.7080 have been reported for the Sete Lagoas Formation (Misi & Veizer 1998; Misi *et al.*, 2007; Babinski *et al.*, 2007; Kuchenbecker, 2011; Alvarenga *et al.*, 2014, Paula-Santos *et al.*, 2015). The latter authors suggest that the difference between the low radiogenic $^{87}Sr/^{86}Sr$ ratios commonly obtained for Bambuí Group and the ratios presented for the late Neoproterozoic (Melezhik *et al.*, 2001; Halverson *et al.*, 2010; Kuznetsov *et al.*, 2013) may be due to the fact that carbonates of the Sete Lagoas Formation have been deposited in a restricted epi-continental sea, and its isotopic composition was not homogenized with contemporary global oceans (Paula-Santos *et al.*, 2015). Silva-Tamayo *et al.* (2010) propose that the Ca isotopic signature recorded in the Sete Lagoas Formation is post-Sturtian with $\delta^{44}Ca$ values ranging from 0 to 1.0‰, which is very different of post-Marinoan cap carbonates that present $\delta^{44}Ca$ values varying between 0 and 2.0‰. However, Kasemann *et al.* (2014) demonstrate that Ca isotopic variations may arise from local depositional processes and, therefore, Ca isotopes would be unsuitable for global correlation. The many differences of interpretation derived from different isotopic methods show that the comparison of Sr and Ca isotope data of the Bambuí Group with global isotopic curves might be inadequate.

Study area

The study area is located in the Southern part of the São Francisco Basin, at the central portion of Minas Gerais state (MG), to the North of Belo Horizonte, between the Sete Lagoas and Vespasiano towns (Fig. 1). The lower Sete Lagoas Formation directly overlies the basement rocks and outcrops in a N-S segment that extends from Confins airport to the North. The upper Sete Lagoas Formation crops out mainly at the central part and the Serra de Santa Helena deposits crop out in the North and Southeast of the study area. An occurrence of the Carrancas Formation is found close to the Sete Lagoas city (Figs. 1 and 2). Five stratigraphic sections from Sete Lagoas Formation were described and sampled on the vertical scale. The Inhaúma (IN) and Sete Lagoas (SL) sections are located on the Western edge of the study area, near to Sete Lagoas city; whereas the Haras Veredas (HV) and Funilândia (FN) sections are located in the Northeastern part close to the Funilândia town; and the Linha Verde (LV) section is located on the South side near the Vespasian town (Fig. 1).

The lower sequence sections comprise mainly grey impure limestones and red dolostones (IN, FN, and LV sections – Fig. 3). The IN section is 38 m thick and display clastic deposits of the Carrancas Formation at the base and fine limestones of the Sete Lagoas Formation at the top, although lithologic contact between these units is not observed on the field (Fig. 3). Oligomictic massive diamictites and laminated siltstones represent the clastic deposits. The diamictites present around 60% of nonlaminated matrix (silt and clay fractions), 35% of clastic angular quartz, granite feldspars (granules) and fragments rocks (granite pebbles), and 5% of carbonate cement and oxides (Fig. 4b). The limestones of IN section are very fine carbonates (microspar) and present flat parallel lamination and low angle cross-lamination, with some primary dolomitic carbonate beds, small aragonite crystals pseudomorphs, and thin clay layers with flame microstructures (Fig. 4a). Some limestones present sub-angular siliciclastic grains (~6%) in silt fraction, mainly composed by monocrystalline quartz and feldspar (Fig. 4a).

The FN section is 35 m thick, with ~16 m covered section, and displays deformed impure limestones and dolostones, micaceous shales (sericite/chlorite), and interlayered clays and oxides (Fig. 3). At the base of the section, there are impure dolostones with apparent parallel flat lamination and shales usually associated with post-depositional tectonic structures, such as local thrust folds and faults, mineral recrystallization, and calcite veins. At the top, less impure limestones with parallel flat lamination and low angle cross-lamination are composed of 80% carbonates (sparite) and 20% of detrital minerals (mainly mono- and poly-crystalline quartz grains) in silt and coarse sand fractions. Clays, detrital micas, and oxides also occur (Fig. 4c). In this section, carbonate samples were collected in ~50 cm intervals (Fig. 3).

The LV section is 10 m thick, with deformed and recrystallized red dolostones and gray impure limestones with apparent flat lamination and low angle cross-lamination (Fig. 3). These rocks are mainly composed of 70% carbonates (sparite and microsparite), but they are fairly recrystallized so the original granulometry is not certain. Quartz grains in silt and fine sand fractions, and interbedded clays represent around 30% of the detrital components (Fig. 4d). Some carbonates show locally deformed chlorite micas suggesting low-grade metamorphism associated with calcite recrystallization and quartz veins that indicate fluids percolation into the carbonate strata (Fig. 4d). These pieces of evidence clearly show post-depositional alteration processes affecting carbonate rocks from FN and LV sections. In addition, the percentage of siliciclastic sediments (quartz and feldspar grains, clays and micas) within the carbonate matrix is ca. 30-20% in LV and FN sections, decreasing to 6% in IN section.

Fine black pure limestones characterize the upper sequence sections (SL and HV sections – Fig. 3). The SL section is 46 m thick and displays black to dark gray organic-rich limestones with parallel flat lamination. These pure carbonates consist of microspar (99%) and detrital components (1%) represented by small grains of quartz and feldspars in silt and
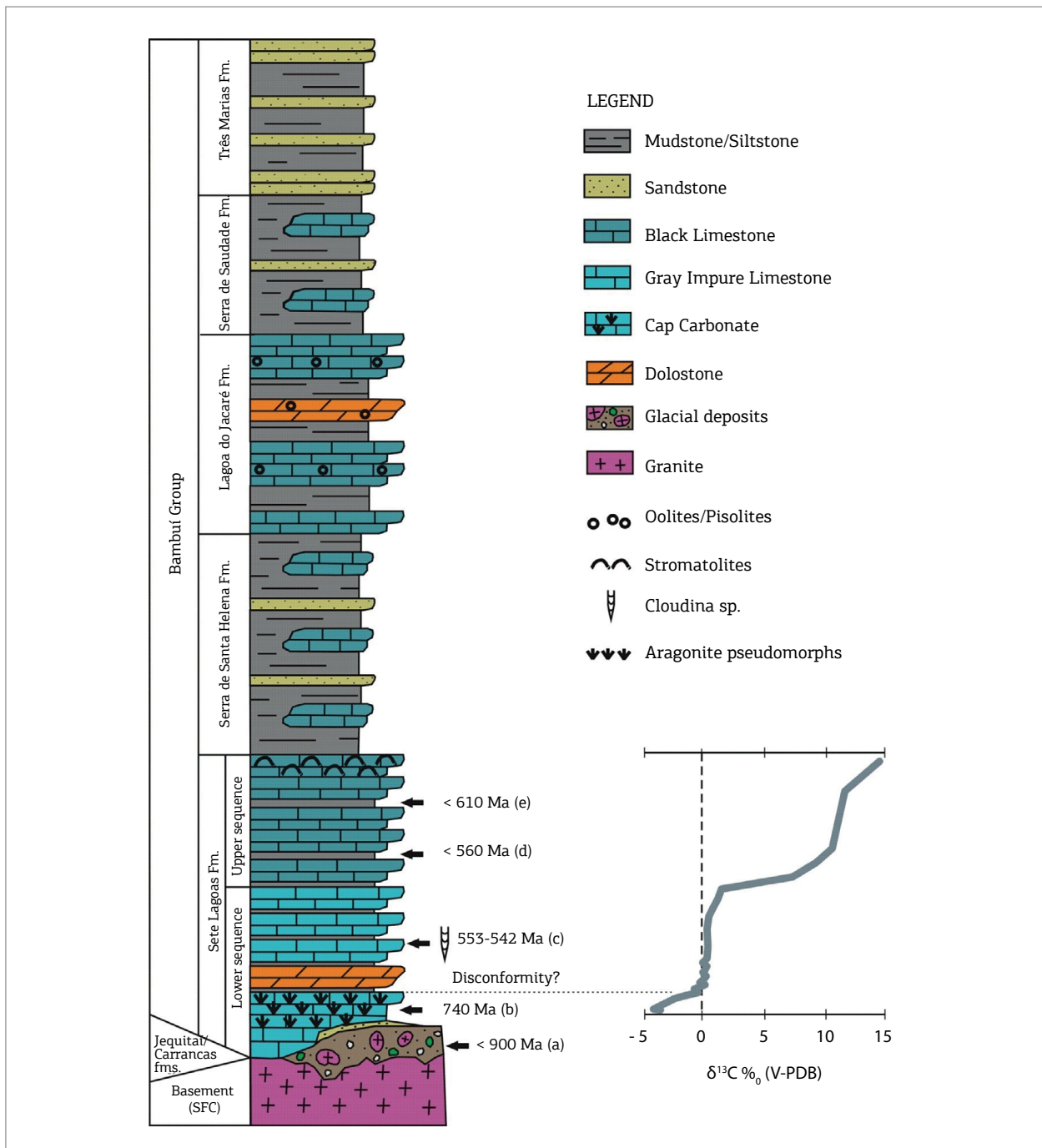
Figure 2. Stratigraphic column of the Bambuí Group according to Dardenne (1978) showing δ¹³C isotopic profile of the Sete Lagoas Formation from Vieira *et al.* (2007) and ages presented from: (A) Buschwaldt *et al.* (1999); (B) Babinski *et al.* (2007); (C) Warren *et al.* (2014); (D) Rodrigues (2008); (E) Paula-Santos *et al.* (2015).

fine sand fractions. Oxide cement associated with stylolite, mineral recrystallization and calcite veins between 0.1 and 1 mm thick is observed at some levels of the section (Fig. 4e). The HV section is 48 m thick and shows gray pure limestones with parallel flat lamination and low angle cross lamination, including calcite nodules and marls intercalated in

the carbonates at the base (Fig. 3). These rocks are composed mainly of microspar (80%) and sparite (18%), with some levels of recrystallized carbonates (Fig. 4f). The detrital components occur in small proportion (2%), represented by quartz and feldspar grains in silt and fine sand fractions. Iron oxides associated with stylolite also occur.
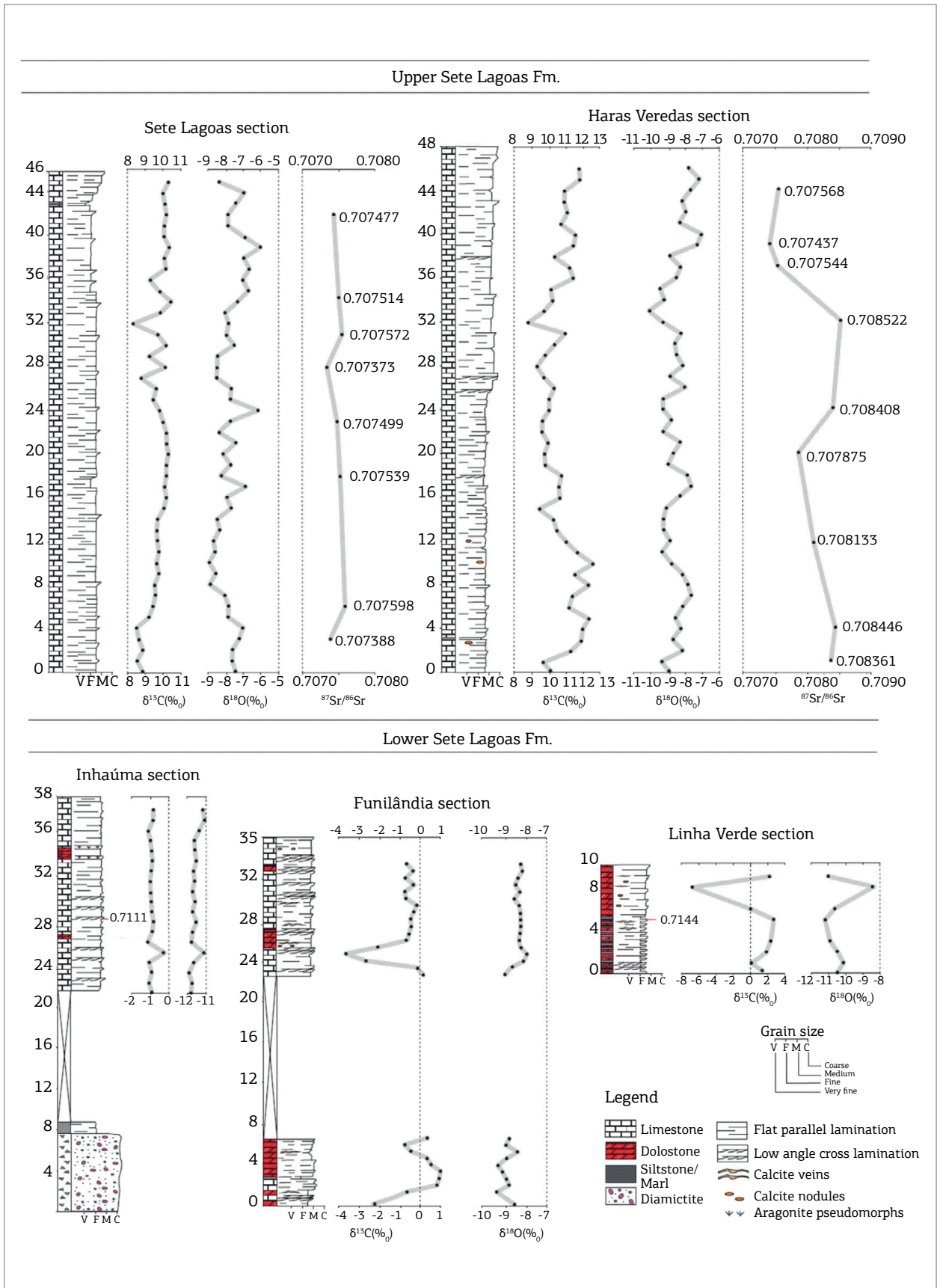
Figure 3. Stratigraphic sections from lower and upper Sete Lagoas Formation with C, O and Sr isotopic profiles.
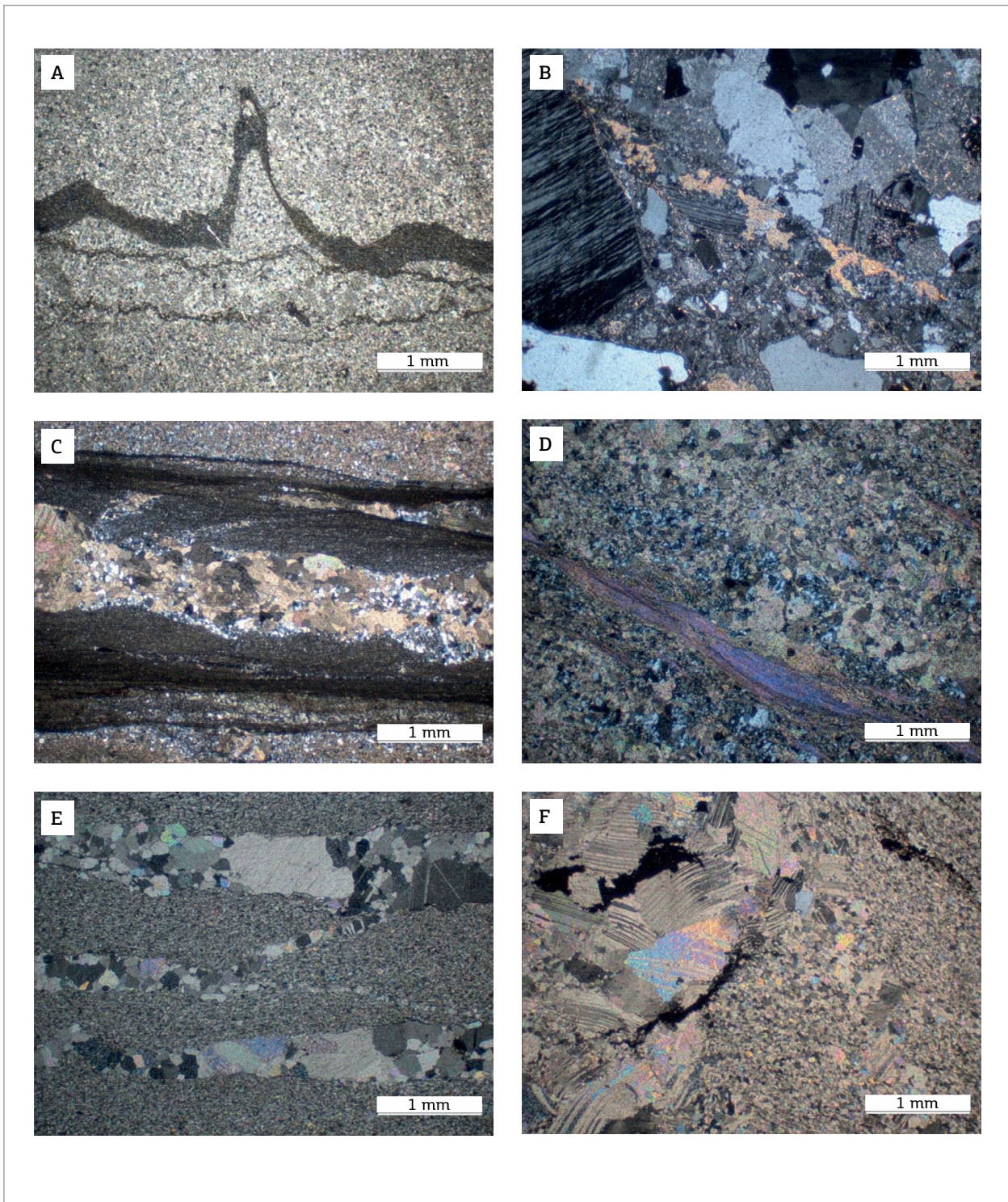
Figure 4. Petrographic photos of the Sete Lagoas and Carrancas formations. (A) Fine limestones with thin clay layers and flame microstructures from Inhaúma section (sample IN-02). (B) Oligomictic massive diamictites showing angular quartz, feldspars and granitic rock fragments within fine matrix, carbonate cement and oxides from the base of Inhaúma section. (C) Impure limestones with interbedded clay layers, detrital sediments and oxides from Funilândia section (sample FN-15). (D) Recrystallized dolostones and impure limestones with interbedded clay layers, detrital sediments and locally deformed chlorite mica from Linha Verde section (sample LV-01). (E) Pure fine limestones (esparite) with calcite veins from the Sete Lagoas section (sample SL-18). (F) Pure limestones with some recrystallized carbonates and iron oxides cement from Haras Veredas section (sample HV-14). Scale bar 1 mm long.

MATERIALS AND METHODS

For this paper, 151 carbonate samples were collected from five sections with vertical intervals of ~1 m (except for FN section that each 0.5 m was sampled) for geochemical and isotopic analyses of C, O, and Sr – the analytical procedures are further described.

Carbonate samples were described after the observation of polished rock and petrographic microscope to recognition of lithology, primary depositional structures and sedimentary facies, and identification of post-depositional structures. Analysis of major elements oxides content was determined by melting the sample with lithium metaborate/tetraborate and subsequent dissolving it with dilute nitric acid. It was then analyzed through Inductively Coupled Plasma Optical Emission Spectrometry (ICP-OES), whereas the trace elements were determined after sample dissolution with aqua regia followed by ICP-MS analysis at the Acme Laboratory. For the isotopic analysis, in each carbonate sample, the most homogeneous possible area without veins, veinlets, minerals recrystallization and stylolite after evaluation under petrographic and/or binocular microscope was selected. In these areas, the material for C, O and Sr isotopic analyses was collected through the micro-drilling technique with small tungsten drills. This procedure helps minimizing or even eliminating the influence of post-depositional alteration in the powdered carbonate, increasing the reliability of the results as a seawater representation at the deposition time. C and O isotope analysis was carried out by means of the powdered sample reaction with 100% heated and manipulated H_3PO_4 in a GasBench II by a mechanical arm. The CO_2 released was analyzed in the isotopic ratio mass spectrometer (IRMS) Delta V Advantage of the *Centro de Pesquisas Geocronólogicas* (CPGeo) at the University of São Paulo. The $\delta^{13}C$ and $\delta^{18}O$ values are reported in V-PDB (Vienna – Pee Dee Bellemnite), with analytical error of ± 0.05‰ for $\delta^{13}C$ and ± 0.07‰ for $\delta^{18}O$ values.

For the Sr isotope analysis, carbonate samples with high Sr concentrations (> 300 ppm when possible) were selected in accordance with Halverson *et al.* (2007). The $^{87}Sr/^{86}Sr$ ratios were obtained by leaching about 100 mg of carbonate, acquired in the micro-drill process, with 2 mL of 0.1N HCl, for one hour. The supernatant was removed, and the sample was centrifuged and washed three times with MilliQ water to obtain the first leaching, which was discarded. Subsequently, 1.4 mL of 1N HCl were added to the dried sample and, after 30 minutes, it reacted. Again, the sample was centrifuged and washed three times; this solution is the second leached, subjected to Sr purification process by ion exchange chromatography technique. $^{87}Sr/^{86}Sr$ ratios were obtained in the TRITON mass spectrometer of the CPGeo at the University of São Paulo, and were normalized to the $^{86}Sr/^{88}Sr$ value of 0.1194. The average

amount of the $^{87}Sr/^{86}Sr$ ratios of the NBS-987 standard determined during this study was 0.710260 ± 0.000040.

RESULTS

C and O isotope data of carbonate samples are presented in Table 1, and geochemical and Sr isotope data are shown in Table 2.

Only two samples of the lower Sete Lagoas Formation were analyzed for Sr isotopes, the IN-08 and LV-06 samples from IN and LV sections, respectively. Petrographic and geochemical data of this portion showed limestones and dolostones with high terrigenous content and low Sr concentrations. Limestones from IN section display consistent $\delta^{13}C$ values, varying between -1.12 and -0.33‰, and $\delta^{18}O$ values between -11.91 and -11.1‰ (Table 1). The IN-08 sample presents a very high radiogenic $^{87}Sr/^{86}Sr$ ratio of 0.711125 ± 0,000035, a low Sr concentration of 249 ppm and geochemical ratios of Rb/Sr = 0.078, Mn/Sr = 1.24, Fe/Sr = 21.04 and Ca/Sr = 1345 (Table 2). Otherwise, $\delta^{13}C$ values of dolostones from LV section are positive with large fluctuations between +0.09 and +2.74‰, and $\delta^{18}O$ values from -11.17 to -10.12‰. Moreover, one negative $\delta^{13}C$ value of -6.73‰ and respective $\delta^{18}O$ of -8.29‰ is observed at the 8-m height of the section (Fig. 3, Table 1). The LV-06 sample presents a very high radiogenic $^{87}Sr/^{86}Sr$ ratio of 0.714395 ± 0,000056, low Sr content of 340 ppm and Rb/Sr of 0.088, Mn/Sr of 1.59, Fe/Sr of 28.0, and Ca/Sr of 853 (Table 2). In addition, $\delta^{13}C$ values of dolostones and dolomitic limestones from FN are very fluctuating at the base and middle parts of the section, between -3.52 and +0.94‰, and $\delta^{18}O$ values range between -9.46 and -7.93‰. However, at the top of the section, the $\delta^{13}C$ values are more consistent, ranging in a narrow interval between -0.76 and -0.19‰, and $\delta^{18}O$ values between -8.50 and -8.19‰ (Fig. 3). Samples from FN section were not analyzed for Sr isotopes, since the FN-12 sample shows a low Sr concentration of 277 ppm and Rb/Sr = 0.064, Mn/Sr = 3.63, Fe/Sr = 20.7, and Ca/Sr = 1029 (Table 2).

On the other hand, carbonates from upper Sete Lagoas Formation were subjected to extensive geochemical and Sr isotopic analysis due to their low terrigenous content and degree of post-depositional alteration. Limestones from SL section show homogeneous and very positive $\delta^{13}C$ values ranging from +8.5 to +10.6‰, with a slight increase from the bottom to top, as well as some fluctuations. The $\delta^{18}O$ values range between -8.8 and -6.0‰ (Fig. 3, Table 1). These limestones have homogeneous and low radiogenic $^{87}Sr/^{86}Sr$ ratios varying between 0.7073 and 0.7076 (Fig. 3), with high and variable content of Sr between 971 and 4,487 ppm, Rb/Sr ≤ 0.007, Mn/Sr < 0.2, Fe/Sr < 1.1 and Ca/Sr < 410 (Table 2).

Table 1. δ¹³C and δ¹⁸O values (‰) of carbonate samples from Sete Lagoas Formation.

Section	Sample	Height (m)	Lithology	δ¹³C	δ¹⁸O	Section	Sample	Height (m)	Lithology	δ¹³C	δ¹⁸O
Inhaúma	IN-01	0.0	Limestone	-0.94	-11.85	Funilândia	FN-06	5.0	Dolostone	0.36	-8.88
	IN-02	1.0	Limestone	-1.01	-11.76		FN-07	25.0	Limestone	0.08	-8.95
	IN-03	2.0	Limestone	-0.95	-11.91		FN-07a	25.5	Limestone	-0.19	-8.68
	IN-04	3.0	Limestone	-1.02	-11.69		FN-08	26.0	Limestone	-2.53	-8.04
	IN-05	4.0	Limestone	-0.33	-11.1		FN-08a	26.5	Limestone	-3.52	-7.93
	IN-06	5.0	Dolostone	-1.12	-11.8		FN-09	27.0	Dolostone	-1.91	-8.27
	IN-07	6.0	Limestone	-0.93	-11.76		FN-09a	27.5	Dolostone	-0.62	-8.36
	IN-08	7.0	Limestone	-0.88	-11.54		FN-10	28.0	Dolostone	-0.54	-8.3
	IN-09	8.0	Limestone	-0.95	-11.72		FN-10a	28.5	Dolostone	-0.46	-8.24
	IN-10	9.0	Limestone	-0.95	-11.62		FN-11	29.0	Limestone	-0.44	-8.22
	IN-11	10.0	Limestone	-0.97	-11.74		FN-11a	29.5	Limestone	-0.34	-8.24
	IN-12	11.0	Limestone	-1.01	-11.64		FN-12	30.0	Limestone	-0.19	-8.29
	IN-13	12.0	Dolostone	-0.97	-11.67		FN-12a	30.5	Limestone	-0.69	-8.5
	IN-14	13.0	Dolostone	-0.9	-11.56		FN-13	31.0	Limestone	-0.76	-8.28
	IN-15	14.0	Limestone	-0.93	-11.61		FN-13a	31.5	Limestone	-0.37	-8.48
	IN-16	15.0	Limestone	-0.98	-11.66		FN-14	32.0	Limestone	-0.71	-8.39
	IN-17	16.0	Limestone	-1.1	-11.39		FN-14a	32.5	Limestone	-0.4	-8.19
	IN-18	17.0	Limestone	-0.81	-11.1		FN-15	33.0	Dolostone	-0.63	-8.27
	IN-19	18.0	Limestone	-0.85	-11.2	Sete Lagoas	SL-01	0.0	Limestone	8.89	-7.49
Linha Verde	LV-01	0.0	Dolostone	1.89	-10.46		SL-02	1.0	Limestone	8.53	-7.58
	LV-02	1.0	Dolostone	0.09	-10.12		SL-03	2.0	Limestone	8.88	-7.54
	LV-03	2.0	Dolostone	1.79	-10.43		SL-04	3.0	Limestone	8.63	-7.14
	LV-04	3.0	Dolostone	2.3	-10.86		SL-05	4.0	Limestone	8.51	-6.96
	LV-06	5.0	Dolostone	2.74	-11.17		SL-06	5.0	Limestone	9.2	-7.81
	LV-07	6.0	Dolostone	0.18	-10.56		SL-07	6.0	Limestone	9.46	-7.75
	LV-09	8.0	Dolostone	-6.73	-8.29		SL-08	7.0	Limestone	9.53	-7.97
	LV-10	9.0	Dolostone	2.29	-10.93		SL-09	8.0	Limestone	9.57	-8.81
Funilândia	FN-01	0.0	Dolostone	-2.24	-8.61		SL-10	9.0	Limestone	9.79	-8.45
	FN-02	1.0	Dolostone	-0.62	-9.46		SL-11	10.0	Limestone	9.65	-8.85
	FN-02a	1.5	Limestone	0.74	-8.84		SL-12	11.0	Limestone	9.78	-8.52
	FN-03a	2.5	Dolostone	0.94	-9.15		SL-13	12.0	Limestone	9.72	-8.56
	FN-04	3.0	Dolostone	0.55	-9.33		SL-14	13.0	Limestone	9.76	-8.2
	FN-04a	3.5	Dolostone	0.32	-9		SL-15	14.0	Limestone	9.78	-8.4
	FN-05	4.0	Dolostone	-0.43	-8.45		SL-16	15.0	Limestone	10.09	-7.6
	FN-05a	4.5	Dolostone	-0.74	-8.95		SL-17	16.0	Limestone	10.17	-7.87
							SL-18	17.0	Limestone	10.09	-6.82

Table 1. Continuation.

Section	Sample	Height (m)	Lithology	δ¹³C	δ¹⁸O	Section	Sample	Height (m)	Lithology	δ¹³C	δ¹⁸O
Sete Lagoas	SL-19	18.0	Limestone	10.12	-8.2	Haras Veredas	HV-11	10.0	Limestone	12.77	-9.07
	SL-20	19.0	Limestone	10.23	-7.59		HV-12	11.0	Limestone	11.66	-9.3
	SL-21	20.0	Limestone	10.35	-8.02		HV-13	12.0	Limestone	11.03	-8.86
	SL-22	21.0	Limestone	10.26	-7.34		HV-14	13.0	Limestone	10.49	-9.22
	SL-23	22.0	Limestone	10.28	-8.28		HV-15	14.0	Limestone	10.3	-9.21
	SL-24	23.0	Limestone	10.09	-6.62		HV-16	15.0	Limestone	9.45	-9.03
	SL-25	24.0	Limestone	9.84	-6.02		HV-17	16.0	Limestone	10.65	-8.36
	SL-26	25.0	Limestone	9.55	-7.63		HV-18	17.0	Limestone	10.6	-7.58
	SL-27	26.0	Limestone	9.7	-7.56		HV-19	18.0	Limestone	10.71	-7.86
	SL-28	27.0	Limestone	8.88	-8.38		HV-20	19.0	Limestone	9.81	-8.91
	SL-29	28.0	Limestone	10.22	-8.36		HV-21	20.0	Limestone	9.76	-8.65
	SL-30	29.0	Limestone	9.3	-8.34		HV-22	21.0	Limestone	9.97	-8.26
	SL-31	30.0	Limestone	10.27	-7.39		HV-23	22.0	Limestone	9.59	-9.2
	SL-32	31.0	Limestone	9.83	-7.83		HV-24	23.0	Limestone	9.65	-8.78
	SL-33	32.0	Limestone	8.34	-7.71		HV-25	24.0	Limestone	10.02	-9.2
	SL-34	33.0	Limestone	9.89	-7.97		HV-26	25.0	Limestone	10.09	-9.25
	SL-35	34.0	Limestone	10.52	-7.23		HV-27	26.0	Limestone	10.37	-7.98
	SL-36	35.0	Limestone	9.83	-6.59		HV-28	27.0	Limestone	9.75	-8.88
	SL-37	36.0	Limestone	9.36	-6.92		HV-29	28.0	Limestone	9.36	-8.08
	SL-38	37.0	Limestone	10.24	-6.51		HV-30	29.0	Limestone	9.82	-9.44
	SL-39	38.0	Limestone	10.15	-6.83		HV-31	30.0	Limestone	10.36	-9.54
	SL-40	39.0	Limestone	10.4	-5.94		HV-32	31.0	Limestone	10.96	-8.26
	SL-41	40.0	Limestone	10.14	-6.77		HV-33	32.0	Limestone	8.82	-9.25
	SL-42	41.0	Limestone	10.14	-7.71		HV-34	33.0	Limestone	9.74	-10.05
	SL-43	42.0	Limestone	10.28	-7.72		HV-35	34.0	Limestone	10.28	-9.17
	SL-45	44.0	Limestone	10.05	-6.78		HV-36	35.0	Limestone	10.16	-9.37
	SL-46	45.0	Limestone	10.4	-8.22		HV-37	36.0	Limestone	11.5	-8.45
Haras Veredas	HV-01	0.0	Limestone	10.16	-8.83		HV-38	37.0	Limestone	11.21	-8.18
	HV-02	1.0	Limestone	9.65	-9.32		HV-39	38.0	Limestone	10.4	-8.85
	HV-03	2.0	Limestone	11.21	-8.07		HV-40	39.0	Limestone	11.47	-7.37
	HV-04	3.0	Limestone	11.47	-8.97		HV-41	40.0	Limestone	11.58	-6.95
	HV-05	4.0	Limestone	11.66	-8.49		HV-42	41.0	Limestone	10.76	-8.29
	HV-06	5.0	Limestone	11.98	-8.57		HV-43	42.0	Limestone	11.12	-7.93
	HV-07	6.0	Limestone	10.87	-8.65		HV-44	43.0	Limestone	10.98	-8.04
	HV-08	7.0	Limestone	11.19	-7.8		HV-45	44.0	Limestone	10.97	-7.6
	HV-09	8.0	Limestone	12.33	-8.42		HV-46	45. 0	Limestone	11.82	-7.04
	HV-10	9.0	Limestone	11.35	-8.42		HV-47	46.0	Limestone	11.8	-7.7

Note: analytical accuracy for: δ¹³C ± 0.05‰ and δ¹⁸O ± 0.07‰.

Limestones from HV section show very positive $\delta^{13}C$ values, between +8.82 and +12.77‰, with the more positive values at the base; and $\delta^{18}O$ values fluctuate between -9.54 and -6.95‰ (Fig. 3, Table 1). These carbonates exhibit variable and highly radiogenic $^{87}Sr/^{86}Sr$ ratios of ~0.7084 at the base, decreasing to 0.7078 in the intermediate part, which later change to ~0.7086 and reduce again to 0.7074 at the top

of the sequence. High Sr concentrations between 1,685 and 2,789 ppm, Rb/Sr ≤ 0.005, Mn/Sr < 0.2, Fe/Sr < 0.9 and Ca/Sr < 240 are recorded in these limestones (Table 2).

DISCUSSION

Table 2. Major elements, Rb and Sr concentrations, geochemical ratios and Sr isotopic data of carbonate samples from the Sete Lagoas Formation.

Sample	Height (m)	Si (%)	Al (%)	Mn (%)	Mg (%)	Ca (%)	Na (%)	K (%)	Fe (%)
LV-06	5.0	8.49	1.74	0.05	0.76	29.04	0.38	0.58	0.95
FN-12	31.0	10.27	1.35	0.1	0.63	28.52	0.3	0.37	0.57
IN-08	7.0	4.02	0.92	0.03	1.44	33.54	< 0.01	0.37	0.52
HV-02	1.0	0.23	0.04	0.02	0.19	39.4	< 0.01	< 0.01	0.03
HV-05	4.0	0.57	0.13	< 0.01	0.21	39	< 0.01	0.06	0.09
HV-11	10.0	2.4	0.35	0.01	0.31	37.21	< 0.01	0.18	0.17
HV-13	12.0	0.29	0.06	0.02	0.21	39.29	< 0.01	0.01	0.06
HV-21	20.0	0.21	0.01	0.02	0.16	39.61	< 0.01	< 0.01	0.03
HV-25	24.0	0.09	< 0.01	0.02	0.17	39.76	< 0.01	< 0.01	0.03
HV-33	32.0	0.13	< 0.01	0.02	0.17	39.5	< 0.01	< 0.01	0.06
HV-38	37.0	0.06	< 0.01	0.02	0.18	39.64	< 0.01	< 0.01	< 0.03
HV-40	39.0	0.06	< 0.01	0.02	0.14	39.52	< 0.01	< 0.01	< 0.03
HV-45	44.0	0.07	< 0.01	0.02	0.16	39.7	< 0.01	< 0.01	< 0.03
SL-04	3.0	0.09	0.03	< 0.01	0.26	39.76	< 0.01	< 0.01	< 0.03
SL-07	6.0	2.16	0.32	0.02	0.24	37.34	0.01	0.15	0.22
SL-10	9.0	0.51	0.17	< 0.01	0.22	38.72	0.01	0.06	0.1
SL-11	10.0	0.59	0.13	< 0.01	0.24	38.77	0.02	0.04	0.08
SL-17	16.0	0.16	0.06	< 0.01	0.17	39.54	< 0.01	0.02	0.03
SL-19	18.0	0.08	0.03	< 0.01	0.11	39.66	< 0.01	< 0.01	< 0.03
SL-21	20.0	0.13	0.06	< 0.01	0.08	39.45	0.01	< 0.01	0.05
SL-24	23.0	0.22	0.07	< 0.01	0.09	39.4	0.02	< 0.01	0.04
SL-28	27.0	0.07	0.01	0.02	0.24	39.62	< 0.01	< 0.01	0.04
SL-29	28.0	0.02	0.04	< 0.01	0.15	39.74	< 0.01	< 0.01	0.04
SL-30	29.0	0.09	0.04	< 0.01	0.17	39.67	< 0.01	0.01	0.05
SL-32	31.0	0.83	0.23	< 0.01	0.22	38.54	0.05	0.08	0.15
SL-33	32.0	0.54	0.3	0.01	0.17	38.67	< 0.01	0.16	0.17
SL-34	33.0	0.72	0.31	< 0.01	0.21	38.42	0.02	0.16	0.19
SL-43	42.0	0.33	0.09	< 0.01	0.11	39.18	0.02	0.02	0.05

Table 2. Continuation.

Sample	Rb (ppm)	Sr (ppm)	Mg/Ca	Rb/Sr	Mn/Sr	Fe/Sr	Ca/Sr	$^{87}Sr/^{86}Sr$	Error
LV-06	30.1	340	0.03	0.088	1.59	28	853	0.714395	0.000056
FN-12	17.8	277	0.02	0.064	3.63	20.7	1029	n.a	n.a
IN-08	19.4	249	0.04	0.078	1.24	21	1345	0.711125	0.000035
HV-02	1.1	1931	< 0.01	0.001	0.12	0.18	204	0.708361	0.000034
HV-05	3.9	2788	0.01	0.001	0.03	0.33	134	0.708446	0.000045
HV-11	11.1	2137	0.01	0.005	0.04	0.82	174	n.a	n.a
HV-13	1.2	2560	0.01	< 0.001	0.06	0.22	153	0.708133	0.000035
HV-21	0.4	2492	< 0.01	< 0.001	0.09	0.14	159	0.707875	0.00004
HV-25	< 0.1	1685	< 0.01	< 0.001	0.14	0.17	236	0.708408	0.000036
HV-33	< 0.1	2075	< 0.01	< 0.001	0.07	0.27	190	0.708522	0.000041
HV-38	0.2	2099	< 0.01	< 0.001	0.07	0.13	189	0.707544	0.000047
HV-40	0.2	2199	< 0.01	< 0.001	0.07	0.13	180	0.707437	0.00004
HV-45	0.2	2008	< 0.01	< 0.001	0.08	0.14	198	0.707568	0.000055
SL-04	1.2	2602	0.01	< 0.001	0.03	0.11	153	0.707388	0.000056
SL-07	10.6	2085	0.01	0.005	0.07	1.04	179	0.707598	0.00004
SL-10	6.1	3160	0.01	0.002	0.02	0.33	123	n.a	n.a
SL-11	5.4	2756	0.01	0.002	0.03	0.3	141	n.a	n.a
SL-17	1.7	2757	< 0.01	0.001	0.03	0.1	143	n.a	n.a
SL-19	0.5	2639	< 0.01	< 0.001	0.03	0.11	150	0.707539	0.000062
SL-21	1.2	3800	< 0.01	< 0.001	0.02	0.13	104	n.a	n.a
SL-24	0.9	4340	< 0.01	< 0.001	0.02	0.1	91	0.707499	0.000046
SL-28	0.9	971	0.01	0.001	0.16	0.43	408	n.a	n.a
SL-29	1.1	2729	< 0.01	< 0.001	0.03	0.15	146	0.707373	0.000046
SL-30	1.5	2327	< 0.01	0.001	0.03	0.21	171	n.a	n.a
SL-32	6.4	2765	0.01	0.002	0.03	0.53	139	0.707572	0.000053
SL-33	10.5	1558	< 0.01	0.007	0.05	1.08	248	n.a	n.a
SL-34	10.2	2332	0.01	0.004	0.03	0.81	165	0.707514	0.000053
SL-43	1.8	4487	< 0.01	< 0.001	0.02	0.11	87	0.707477	0.000046

Note: n.a.= not analyzed.

C and O isotopic variations

Carbon isotopic chemostratigraphy in marine carbonates has been the most important tool to study the Neoproterozoic sedimentary record, especially in the absence of recognizable fossils or reliable radiometric ages (Kaufman, 1997). However, some carbonates are usually susceptible to post-depositional alterations, especially those of Precambrian age, which change the original isotopic and geochemical seawater record. Recognition of post-depositional alteration processes is extremely important to ensure the reliable application of C isotopic chemostratigraphy (Melezhik *et al.*, 2001). According to Brand and Veizer (1980) and Banner and Hanson (1990), the interaction of carbonates with interstitial fluids during diagenesis, dolomitization or metamorphism leads to an increase in the Rb/Sr, Mn/Sr, Fe/Sr and $^{87}Sr/^{86}Sr$ ratios,

and a decrease in the $\delta^{13}C$ and $\delta^{18}O$ values. Therefore, several authors present many post-depositional alteration geochemical parameters (Asmeron *et al.*, 1991; Derry *et al.*, 1992; Kaufman *et al.*, 1993; Kuznetsov *et al.*, 1997; Semikhatov *et al.*, 1997; Jacobsen & Kaufman, 1999; Folling & Frimmel, 2002; Frimmel, 2010; Kuznetsov *et al.*, 2013). In all cases, such geochemical parameters and their threshold values are empirical. Herein, we have used the threshold parameters of Mn/Sr < 2, Fe/Sr < 50 and $\delta^{18}O$ values > -10‰ (V–PDB) proposed by Fölling and Frimmel (2002) to identify the least altered $\delta^{13}C$ values in the carbonates. These parameters were chosen as they consider different reliability limits for C and Sr isotope and are more rigorous than the others.

In the case of impure limestones and dolostones from LV section, the $\delta^{13}C$ values vary from +2.74 to -6.73‰, $\delta^{18}O$ values range from -8.29 to -11.17‰; and dolomitic limestones from the base of FN section show a similar behavior, with $\delta^{13}C$ values between +0.94 and -3.52‰, and $\delta^{18}O$ values from -7.93 to -9.46‰ (V–PDB). The C and O isotope compositions of these carbonates are very fluctuating and display a negative correlation between them (Fig. 5), suggesting post-depositional alteration related to dolomitization processes, and thus resulting in a decrease of $\delta^{13}C$, as well as an increase in the Mn/Sr and Fe/Sr ratios like suggested by Brand and Veizer (1980). However, Banner and Hanson (1990) proposed that $\delta^{18}O$ values decrease during post-depositional alteration too, but, in this case, the $\delta^{18}O$ values show a behavior of rising (Fig. 5). This correlation can be the result

of fluid-rock interactions when fluids with a different oxygen isotopic composition infiltrate a sediment (i. e. Derry, 2010). Furthermore, the altered carbonates display Mn/Sr and Fe/Sr below the geochemical parameter proposed by Fölling and Frimmel (2002), suggesting that such threshold parameters are not entirely reliable (Fig. 6). Field and petrographic data support the interpretation of dolomitization as the major post-depositional processes affecting these carbonates due to significant occurrences of impure recrystallized dolostones and some limestones, deformed micaceous shales and inter-layered clays and oxides, usually associated with tectonic structures, such as local thrust folds and faults, calcite veins and mineral recrystallization. The post-depositional dolomitization process probably happened during the exhumation and thrust of the Araçuaí Belt on the Southeastern part of the São Francisco Craton, as shown by the association between dolomites and tectonic structures (Guacaneme *et al.*, 2014; Paula-Santos *et al.*, 2015).

On the other hand, fine limestones from IN section and impure limestones from upper FN section present high consistency in the $\delta^{13}C$ values, which vary between -1.0 and 0‰, and $\delta^{18}O$ values between -11.91 and -7.93‰ (V–PDB). These values are interpreted as representative of the depositional environment and can be correlated with those obtained by Santos *et al.* (2004) and Vieira *et al.* (2007b) in carbonates from the first depositional sequence of the Sete Lagoas Formation, which were above the cap carbonate with negative $\delta^{13}C$ values around -4.5‰ and below the positive C isotopic shift (Fig. 5). In addition, these carbon isotopic

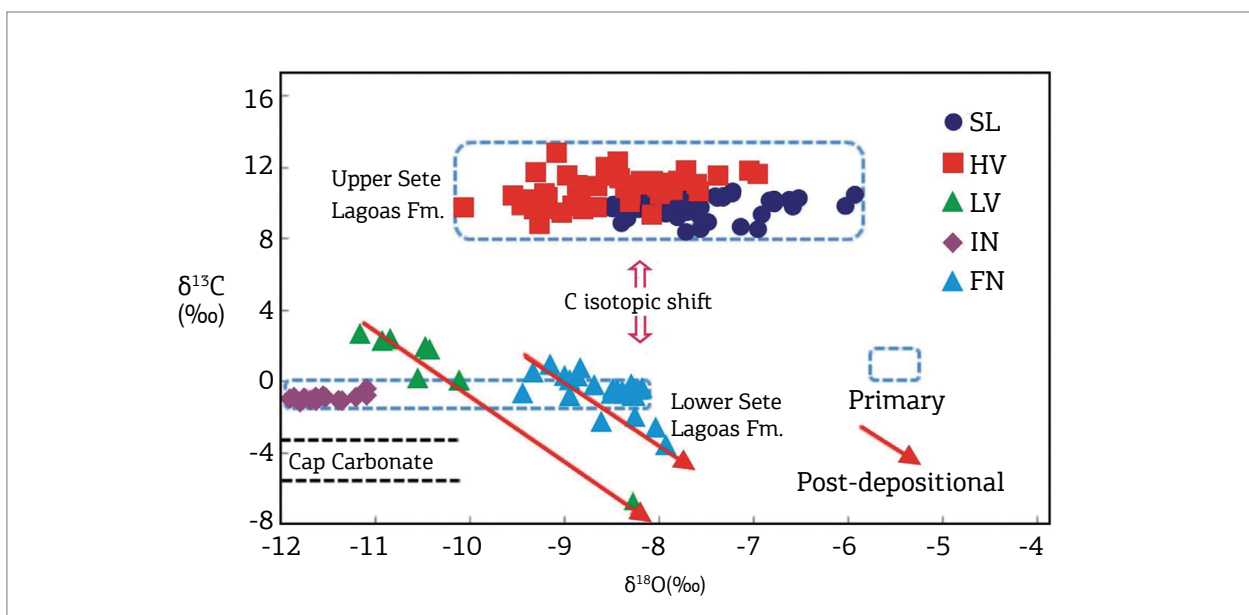Figure 5. $\delta^{13}C$ *vs.* $\delta^{18}O$ diagram of carbonates from lower and upper Sete Lagoas Formation showing major isotopic signatures of depositional (primary) and post-depositional dolomitization processes. Cap carbonate data from Vieira *et al.* (2007a) and Babinski *et al.* (2007) are showed for comparison. Key for different sections is given in Fig. 1.

values are correlated with those obtained by Kuchenbecker (2011), Alvarenga *et al.* (2014), Warren *et al.* (2014) and Paula Santos *et al.* (2015) at the unit base. These carbonates are characterized by sedimentary structures as rhythmic lamination interlayered with pelites, clays and truncated irregular laminations, possibly associated with tidal shallow marine environment, typically attributed to Pedro Leopoldo Member described by Schöll (1976), Ribeiro *et al.* (2003), Vieira *et al.* (2007a, b) and Paula-Santos *et al.* (2015), corresponding to the lower Sete Lagoas Formation. The δ^{13}C values around 0‰ are almost constant throughout the lower sequence (above the cap carbonate) and can indicate a steady state system in which there is isotopic mass balance between the input and the removal of carbon through several isotopic fractionation processes. This may reflect a marine environment possibly in equilibrium with the contemporary global oceans.

Upwards, carbonates from SL section show very positive and homogeneous δ^{13}C values ranging between +8.5 and +10.5‰, and δ^{18}O values between -6.0 and -8.8‰. These are well correlated with δ^{13}C values of carbonates from HV section, between +8.8 and +12.6‰, and δ^{18}O values between -7.0 and -9.5‰ (Fig. 5). These data most likely represent the isotopic composition of the depositional environment, due to the high consistency of the δ^{13}C values, in addition to field and petrographic data that display preserved limestones with original sedimentary structures and low degree of post-depositional alteration. The geochemical parameters proposed by Fölling and Frimmel (2002) also point out this interpretation, with Mn/Sr < 0.2, Fe/Sr < 1 and δ^{18}O values > -10‰, below the threshold parameters (Fig. 6). They confirm δ^{13}C values as representative of the isotopic seawater composition at the time of deposition. These isotopic data correlate with

the δ^{13}C values obtained by Santos *et al.* (2004), Vieira *et al.* (2007b) and Paula-Santos *et al.* (2015), which suggest that the SL and HV sections are positioned above the characteristic C isotopic shift from the upper Sete Lagoas Formation (Fig. 5). The primary calcareous sedimentary structures, such as flat parallel lamination and low angle cross lamination indicate a deep marine environment, less affected by the influence of tidal currents or storms. These sedimentological characteristics are similar to those described for the upper part of Sete Lagoas Formation, known as Lagoa Santa Member (Schöll, 1976; Ribeiro *et al.*, 2003). In this second stage of depositional environment evolution of the Sete Lagoas Formation, a second marine transgression with deeper water and less energy took place (Vieira *et al.*, 2007b; Paula-Santos *et al.*, 2015).

The positive δ^{13}C values are common throughout the upper sequence and represent biochemical processes widely distributed inside the marine environment, although the absolute values are somewhat different. This carbon isotopic trend can be explained by various processes, such as increase of high burial rates of organic matter (Knoll *et al.*, 1986); methanogenesis associated with fermentation and direct reduction of CO_2 (Whithicar *et al.*, 1986); sulfate reduction accompanied by sulfide generation under anaerobic conditions (Claypool & Kaplan, 1974; Pierre, 1989); high photosynthetic bio-productivity; high evaporation rates (Frimmel, 2010); and production and distribution of authigenic carbonate (Schrag *et al.*, 2013, 2014). Additionally, carbon isotopes are subject to seasonal variations due to their low residence time in the oceans, of around 433 years (Frimmel, 2010). It is likely that the very positive δ^{13}C record of the upper Sete Lagoas Formation is the result of several processes that can be reflected in local or regional scales.

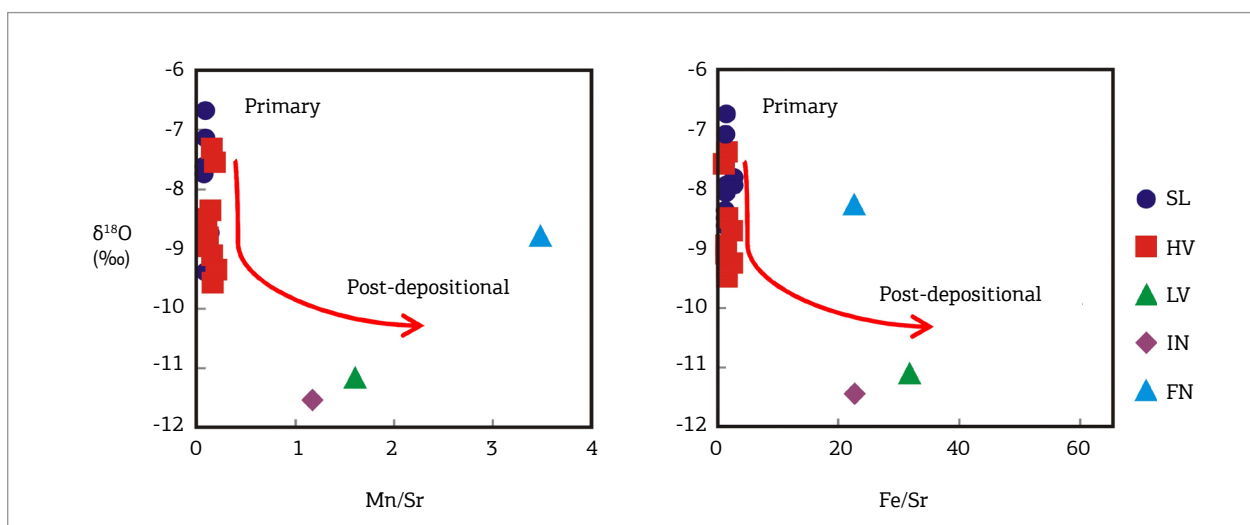Figure 6. δ^{18}O (V-PDB) values *vs.* Mn/Sr and Fe/Sr ratios of carbonates from Sete Lagoas Formation showing isotopic signatures of depositional (primary) and post-depositional trends. Key for different sections is given in Fig. 1.

As pointed out by Santos *et al.* (2000), there are occurrences of natural gas and sulfides suggesting important methanogenesis processes and sulfate reduction, but on a local scale. On a regional scale, the same authors propose that high-C isotopic values are mainly due to ^{12}C fixation through photosynthetic processes and great contribution of restricted basin, as this very positive C isotopic trend is characteristic of the upper Sete Lagoas Formation. Inefficient circulation results in low oxygenation of deep waters, thus favoring preservation of organic matter, which leads to high rates of ^{13}C in the water column. This breaks the situation of steady state that was active in the lower Sete Lagoas Formation and changes all the C isotopic balances of the basin (causing precipitation of carbonates with very positive $\delta^{13}C$). This does not seem to be a global event, because carbonate successions with $\delta^{13}C$ higher than +10‰ are not common (i.e Halverson *et al.*, 2005). Although highly positive carbon isotope excursions in organic-rich limestones and dolostones ($\delta^{13}C >$ +12‰) are reported in Neoproterozoic carbonate successions in Congo (Elandshoek and Hüttenberg Formations) and Kalahari Cratons (Kaufman *et al.*, 2010), correlations to the Bambuí Group are still unclear. The shift observed in the São Francisco Basin occurs above the *Cloudina* sp. fossil, and therefore is most likely younger than the shifts observed in the African units. Additionally, positive C isotope excursions are observed in many episodes during Cryogenian and Ediacaran (see Hebert *et al.*, 2010 for compilation) and cannot blindly be used for correlations, which requires caution.

Sr isotopic variations

To assess post-depositional alteration of Sr isotopes, we have used the threshold of geochemical parameters of Rb/Sr < 0.001, Mn/Sr < 0.5, Fe/Sr < 3 and Ca/Sr < 1,000 proposed by Folling and Frimmel (2002). Carbonates from lower Sete Lagoas Formation are characterized by low Sr content (< 350 ppm) and very high radiogenic $^{87}Sr/^{86}Sr$ ratios (> 0.7111). The geochemical ratios Rb/Sr > 0.060, Mn/Sr > 1.20, Fe/Sr > 20 and Ca/Sr > 850 are above the threshold parameters, suggesting post-depositional alteration of these carbonates. Field and petrographic data that clearly show intense post-depositional dolomitization on the Eastern border of the São Francisco Basin support this interpretation, which modifies the geochemical and isotopic original signature. It is likely that during the dolomitization process, the primary Sr was leachate and radiogenic Sr from interstitial fluids has been incorporated into the chemical structure of carbonates. However, disturbances of Sr isotope composition depend not only on the extent of post-depositional alteration but also on the initial composition of carbonates (Melezhik *et al.*, 2001). Carbonates from lower Sete Lagoas Formation present significant amounts of Si, Al and K, which indicate a contribution of detrital sediments and possibly influence of freshwater

on the carbonate platform. A decrease in such detrital input from East to West was noticed in the studied area, and therefore there was also decrease in the external waters input, which is corroborated by our geochemical data. Whereas FN-12 carbonate sample display Si and Al concentrations of more than 8 and 1%, the IN-08 sample has less than 5 and 1% of Si and Al, respectively. According to Melezhik *et al.* (2009), the presence of siliciclastic particles may also increase the porosity and permeability of the carbonates, thereby making them more vulnerable to infiltration of external fluids. Thus, carbonates enriched in aluminosilicate minerals show variable degrees of post-depositional alteration accompanied by an increase of Mg/Ca and Mn/Sr ratios.

On the other hand, limestones from upper Sete Lagoas Formation present high Sr contents (> 900 ppm), less radiogenic $^{87}Sr/^{86}Sr$ ratios varying between 0.7073 and 0.7086, and Rb/Sr ratios ≤ 0.007, Mn/Sr < 0.2, Fe/Sr < 1.1 and Ca/Sr < 410 (Table 2). The geochemical ratios of these carbonates are below the threshold parameters proposed by Folling and Frimmel (2002), except for the Rb/Sr ratio (> 0.001). These data suggest that the Sr isotope composition represents the depositional environment, and it is not affected by diagenesis or post-depositional processes. The Rb/Sr parameter is not totally reliable in this case, considering the high consistency in the $^{87}Sr/^{86}Sr$ ratios, besides field, petrographic, and geochemical data that show well-preserved pure limestones, with less than 2% of detrital minerals and very low Si and Al contents (< 1%). Therefore, we suggest a specific assessment for each study section at the expenses of geochemical threshold values established in the literature. In this case, Rb/Sr ratio < 0.008 can be established.

Initially, the large variation in the $^{87}Sr/^{86}Sr$ ratios between 0.7073 and 0.7086 obtained in well-preserved limestones from upper Sete Lagoas Formation was interpreted as the result of an interaction of seawater with freshwater on the marine carbonate platform (Guacaneme, 2015). This suggests that carbonates of Sete Lagoas Formation probably have been deposited in a restricted epi-continental sea, like proposed by Paula-Santos *et al.* (2015). Additionally, large variations in the Sr isotope ratios are confined to the Eastern margin of the basin (HV section). Therefore, the isotope record of this sector was investigated in more details. High-resolution Sr isotope data from carbonate samples of HV section, located in the Eastern margin of the study area, exhibit variable low and high radiogenic $^{87}Sr/^{86}Sr$ ratios ranging from 0.7074 to 0.7086, high Sr concentrations between 1,685 and 2,789 ppm and geochemical ratios of Rb/Sr < 0.001, Mn/Sr < 0.15, Fe/Sr < 0.4 and Ca/Sr < 240 (Fig. 7). The radiogenic $^{87}Sr/^{86}Sr$ ratios (> 0.7080) could be interpreted as the effect of continental weathering and riverine high radiogenic Sr input to seawater or during early diagenesis, based on Palmer
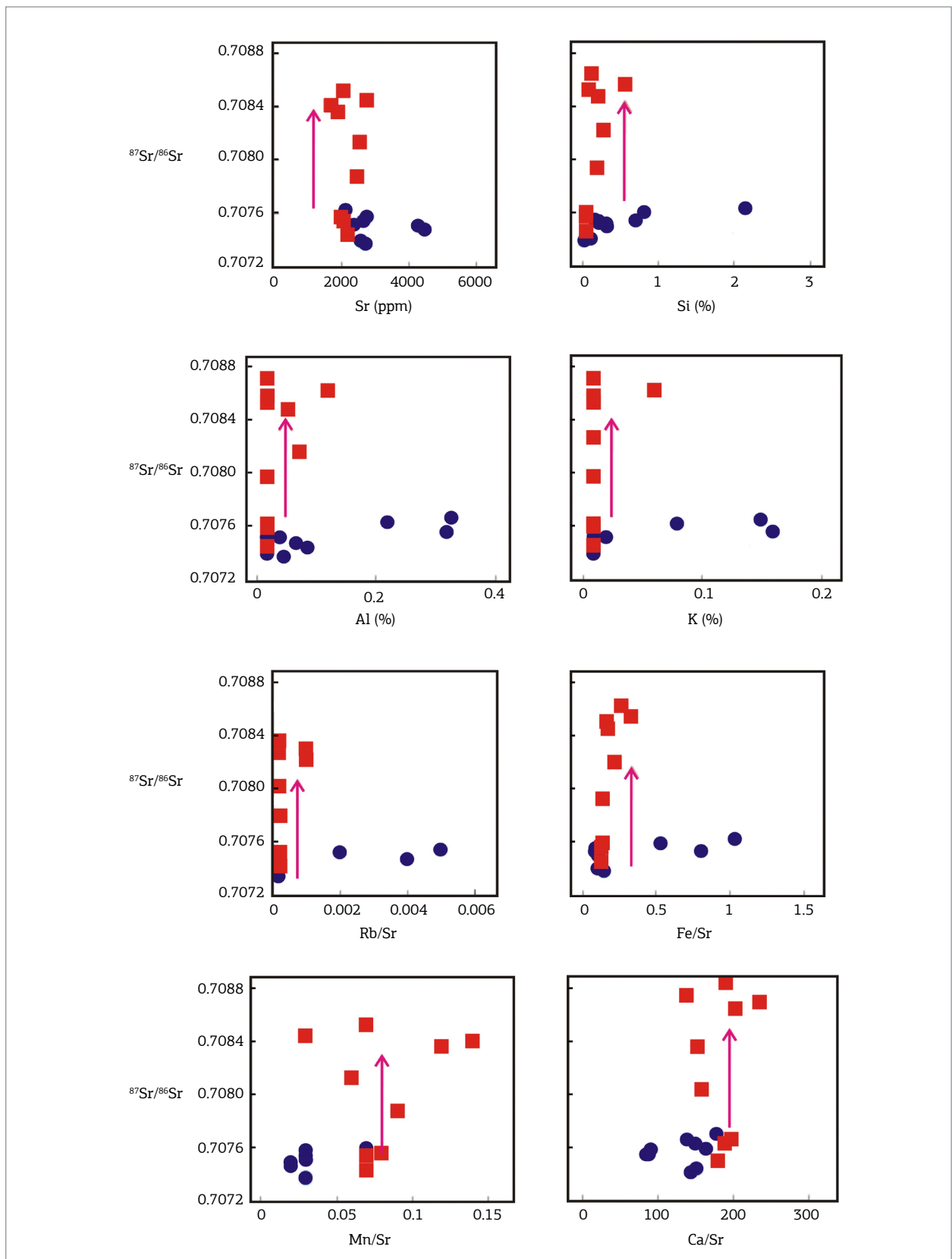
Figure 7. ⁸⁷Sr/⁸⁶Sr ratios *vs.* Sr concentrations, major elements and geochemical ratios of carbonates from Sete Lagoas section (blue circles) and Haras Veredas section (red squares). The red arrows show the influence of SGD on Haras Veredas section.

and Edmond (1989) and Shields (2007), as these carbonates were deposited on the proximal sector of the carbonate platform. However, this hypothesis is not consistent due to the lack of correlation between radiogenic $^{87}Sr/^{86}Sr$ ratios and Si, Al and K contents (Fig. 7), as would be expected for riverine discharge. Therefore, another explanation must be claimed. We assume that the high radiogenic $^{87}Sr/^{86}Sr$ ratios recorded in HV limestones can be a local effect of variable amounts of submarine groundwater discharge (SGD) in this part of the basin. This would explain the high fluctuation in $^{87}Sr/^{86}Sr$ ratios, without correlated detrital input.

Several authors had already investigated the impact of SGD in marine Sr isotope budget (Basu *et al.*, 2001; Dowling *et al.*, 2003; Rahaman & Singh, 2012; Beck *et al.*, 2013). The Sr flux to the ocean from SGD is a major component (13 to 31%) of the marine Sr isotope budget (Beck *et al.*, 2013). However, there is some controversy regarding if groundwater sources are less or more radiogenic relative to $^{87}Sr/^{86}Sr$ seawater composition, which is influenced by both carbonate and silicate weathering, with a negative or positive effect on the SGD $^{87}Sr/^{86}Sr$ ratios. Even so, Beck *et al.* (2013) proposed that global average SGD $^{87}Sr/^{86}Sr$ ratios vary from 0.7083 to 0.7094. In a similar way, the Eastern margin of the São Francisco basin might have also been subject to local isotopic exchange processes of seawater with SGD, incorporating external Sr. While isotope exchange affects the isotopic seawater composition, it does not appear to modify the concentration of Rb, Sr, Si, Al, K and Fe elements (Fig. 6). Therefore, a Sr isotopic local trend dominated by SGD, independent from detrital input, is suggested. In the modern ocean Sr budget, Beck *et al.* (2013) explain that the estimate of the less-radiogenic Sr input by SGD does not appear to be sufficient to balance the radiogenic river source, but it substantially reduces the imbalance. Groundwater input with less radiogenic $^{87}Sr/^{86}Sr$ than seawater buffers the rise in the $^{87}Sr/^{86}Sr$ of seawater caused by the fluvial input of radiogenic Sr, and is comparable in magnitude to the flux driven by submarine hydrothermal circulation through oceanic spreading centers and diagenetic processes. The fact that the SGD-driven Sr flux is a major component of the budget implies that changes in the SGD volume inputs over geologic time may have contributed to temporal variations in marine $^{87}Sr/^{86}Sr$ ratios (Beck *et al.*, 2013). The direct flow of SGD into the ocean and the chemical reactions of meteoric and seawater mixtures within coastal aquifers are processes that have been largely ignored when estimating material flows between land and sea (Moore, 2010). Although in only one sector of the São Francisco Basin, our data from HV section seem to support these observations for the role of SGD in marine basins through time.

Another possibility to explain the variability in the $^{87}Sr/^{86}Sr$ ratios in the HV section would be that the more radiogenic values represent periods of connection of the basin to the contemporaneous global ocean isotope pool, as ratios around 0.7085 would be expected at the Ediacaran-Cambrian boundary (Halverson *et al.*, 2007, 2010; Kuznetsov *et al.*, 2013). However, the limestones from SL section, located in the Western sector of the study area, show homogeneous and low radiogenic $^{87}Sr/^{86}Sr$ ratios varying between 0.7073 and 0.7076, with high and variable contents of Sr between 970 and 4,487 ppm, Rb/Sr ≤ 0.005, Mn/Sr ≤ 0.07, Fe/Sr < 1.1, and Ca/Sr < 180 (Fig. 7). This discrepancy between distal and proximal environments dismisses any possibilities that the more radiogenic ratios in the HV section would represent connection periods to the global ocean; as such event should be recorded at regional scale. Hydrothermal activity of oceanic crust is also unlikely to be a possible source of low radiogenic $^{87}Sr/^{86}Sr$ ratios recorded in these limestones, due to the epi-continental tectonic context of the São Francisco Craton. The great homogeneity in the Sr isotope composition would indicate less influence of freshwater, suggesting that these limestones were deposited on the distal sector of the carbonate platform and preserve the original Sr isotope seawater composition. Moreover, discrepancies in the $^{87}Sr/^{86}Sr$ ratios between distal and proximal environments suggest inefficient circulation in the São Francisco basin at this stage. Finally, the Sr ratios on the deep sectors (devoid of freshwater influence) are much lower than those predicted (higher than 0.7080) for the Ediacaran-Cambrian boundary in many curves of the Sr isotope composition evolution for the global ocean (Halverson *et al.*, 2010; Kuznetsov *et al.*, 2013). A possible explanation for low radiogenic $^{87}Sr/^{86}Sr$ ratios of limestones from SL section is the enhanced carbonate dissolution in the source areas due to uplifting, prevailing over silicate chemical weathering and keeping low radiogenic $^{87}Sr/^{86}Sr$ ratios and high Sr content (Paula-Santos *et al.*, 2015). Carbonate dissolution (calcite, dolomite) and evaporitic sulfates (gypsum, anhydrite) are considered an important source of Sr to the ocean (Brass, 1976) due to the high Sr content and solubility of those minerals. This may have produced a remarkable difference between the $^{87}Sr/^{86}Sr$ ratios of the Bambuí Group and those expected in Sr isotopic curves for the Ediacaran-Cambrian boundary.

Geotectonic considerations and implication for Sr isotope chemostratigraphy

The restricted marine environment hypothesis breaks an important premise for the application of Sr isotope stratigraphy as global correlation tool of the Bambuí Group with other contemporary carbonate sequences. However, we compare the

^{87}Sr/^{86}Sr ratios obtained in this study with the Sr isotope evolution seawater curves during the Neoproterozoic and Cambrian proposed in the literature (Melezhik *et al.*, 2001; Halverson *et al.*, 2007; Kuznetsov *et al.*, 2013). The large variations of the ^{87}Sr/^{86}Sr ratios between 0.7073 and 0.7086 are reported for the Ediacaran and Early Cambrian periods in the Sr isotope evolution of the global ocean reconstructions (Fig. 8), and could suggest the possibility of intermittent connectivity of the oceans during this time interval. In this assumption, partial exchange of water between the Bambuí sea and contemporary oceans would have taken place, allowing Sr isotope seawater homogenization, especially through high radiogenic ^{87}Sr/^{86}Sr ratios > 0.7083 obtained in well-preserved limestones from HV section (Fig. 6). However, these higher ^{87}Sr/^{86}Sr ratios occur only close to the basin margins and not on the deep platform, so the isotopic homogenization does not seem plausible at least for the upper Sete Lagoas Formation. The assumption that the depositional environment of Sete Lagoas Formation was restricted during the Ediacaran-Cambrian period is more reasonable due to the geochemical and isotopic data presented herein. If there was an open marine setting, it might have been set during deposition of the lower part of the unit, where carbonates display steady state situation in the δ^{13}C values around 0‰. The restriction probably caused lack of isotope homogenization between the São Francisco

basin seawater and the global ocean, which may explain the mismatching ^{87}Sr/^{86}Sr ratios obtained in the deeper SL section (~0.7075) and those proposed in several Sr evolution curves for the Neoproterozoic (> 0.7080). This illustrates a case where Sr blind dating is not a reliable tool for temporal positioning of a carbonate succession.

We also note that our geochemical data are in agreement with the geotectonic framework of the São Francisco Basin during the Ediacaran-Cambrian boundary. Slightly impure limestones from IN section show 6% of detrital sediments and low concentrations of Si, Al and K. Therefore, these carbonates may have been deposited in a more distal marine environment (West of the study area), while impure carbonates of LV and FN sections with 20 to 30% of detrital sediments, consisting of small grains of quartz and feldspar in the silt and sand fraction and more content of Si, Al and K suggest that these carbonates were deposited close to the coastline (East), with greater freshwater influence and contribution of continental sediments. Similarly, limestones from HV section, located in the Eastern part of the study area, show Sr isotopic features of proximal environment and influence of freshwater and/or SGD, suggesting that probably a coastline existed in the Eastern part of the basin. This is in agreement with the restricted environment proposed by Paula-Santos *et al.* (2015) during
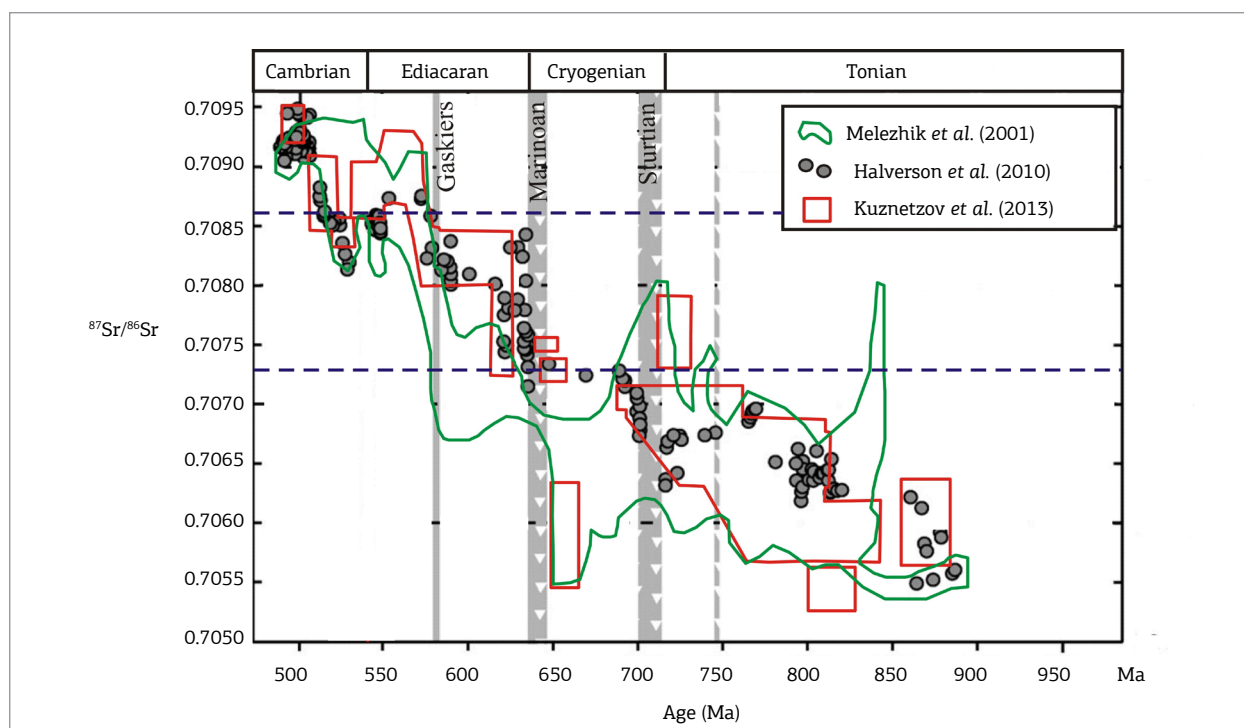

Figure 8. Sr isotope evolution curves of Neoproterozoic and Early Cambrian Global Ocean. Dashed blue lines limit the interval of ^{87}Sr/^{86}Sr ratios obtained in this study. Vertical bars represent global glaciations. Modified from Melezhik *et al.* (2001), Halverson *et al.* (2010) and Kuznetsov *et al.* (2013).

the late Ediacaran, which suggest a proximal source of the study area with strong influence of freshwater from East to West, and contribution of detrital sediments derived from the Araçuaí orogen. It also shows that the Araçuaí orogen would be built on the Eastern border of the São Francisco craton, which is consistent with geochronological data pointing to post-collisional Araçuaí super-suites (Pedrosa-Soares *et al.*, 2011) as representative sources of the Sete Lagoas Formation sediments. Thus, Paula-Santos *et al.* (2015) suggested that the Bambuí Group was deposited in a foreland basin in which a restricted epi-continental sea submerged the São Francisco Craton when the surrounding orogens were completely built.

CONCLUSIONS

Carbonate rocks from Sete Lagoas Formation show lithological, geochemical, and isotopic variations, representing both depositional and post-depositional processes on the carbonate platform. This allows discriminating between impure limestones with low $\delta^{13}C$ values and well-preserved pure limestones with very positive $\delta^{13}C$ values. Therefore, it puts the stratigraphic sections in the lower and upper sequences of the Sete Lagoas Formation, separated by a C isotopic shift that occurs in a regional scale at the São Francisco basin. Some impure limestones and dolostones from the lower sequence display large disturbances on the C, O and Sr isotopic compositions associated with post-depositional dolomitization processes.

The analysis of $^{87}Sr/^{86}Sr$ ratios of well-preserved limestones from upper Sete Lagoas Formation shows important local controls on the basin Sr budget. The large isotopic fluctuations in the $^{87}Sr/^{86}Sr$ ratios on the Eastern border may be the result of seawater interaction with freshwater and SGD flux coming from the continent, suggesting a restricted marine environment. Because the SGD is a major component of the Sr flux to marine budget, it may have implications on the Neoproterozoic and Cambrian seawater composition and may also contribute to temporal variations in $^{87}Sr/^{86}Sr$ ratios of the Bambuí marine basin.

In addition, strong local controls on the Sr ratios suggest that thermohaline circulation homogenization was much less effective in the Bambuí basin than in open marine environments, reinforcing a restricted setting for the Bambuí Group deposition. Such inefficient circulation and restriction probably led to less oxygenated deep waters, preventing oxidation of organic matter. This may have had an important impact on the C isotope budget of the basin, resulting in extremely high $\delta^{13}C$ values on the upper Sete Lagoas Formation.

ACKNOWLEDGMENTS

REFERENCES

Alkmim F.F. & Marshak S. 1998. Transamazonian Orogeny in the southern São Francisco Craton region in Minas Gerais, Brazil: evidence for Paleoproterozoic collision and collapse in the Quadrilátero Ferrífero. *Precambrian Research*, **90:**29-58.

Alkmim F.F., Chemale Jr. F., Endo I. 1996. A deformação das coberturas proterozoicas do Cráton do São Francisco e o seu significado tectônico. *Revista da Escola de Minas*, **49:**22-38.

Alkmim F.F. & Martins-Neto M.A. 2001. A bacia intracratônica do São Francisco: Arcabouço estrutural e cenários evolutivos. In: Pinto, C.P., Martins-Neto, M. (Eds.). *A Bacia do São Francisco geologia e recursos naturais.* SBG, Belo Horizonte, pp. 9-30.

Alkmin F.F., Martins-Neto M.A., 2012. Proterozoic first-order sedimentary sequences of the São Francisco craton, eastern Brazil. *Marine and Petroleum Geology*, **33:**127-139.

Almeida F.F.M. 1977. O Cráton do São Francisco. *Revista Brasileira de Geociências*, **7:**349-364.

Almeida F.F.M., Hasui Y., Brito Neves B.B. 1976. The Upper Precambrian of South America. *Boletim do Instituto de Geociências*, Universidade de São Paulo, **7:**45-80.

Alvarenga C.J.S., Santos R.V., Vieira L.C., Lima B.A.F., Mancini L.H. 2014. Meso-Neoproterozoic isotope stratigraphy on carbonates plataforms in the Brasilia Belt of Brazil. *Precambrian Research*, **251:**164-180.

Asmeron Y., Jacobsen S., Knoll A.H., Butterfield N.J., Swett K. 1991. Strontium isotope variations of Neoproterozoic seawater: implications for crustal evolution. *Geochimica et Cosmochimica Acta*, **55:**2883-2894.

Babinski M., Vieira L.C., Trindade, R.I.F. 2007. Direct dating of Sete Lagoas cap carbonate (Bambuí Group, Brazil) and implications for the Neoproterozoic glacial events. *Terra Nova*, **19:**401-406.

Babinski M., Pedrosa-Soares A.C., Trindade R.I.F., Martins M., Noce C.M., Liu D. 2012. Neoproterozoic glacial deposits from the Araçuaí orogen, Brazil: Age, provenance and correlations with the São Francisco craton and West Congo belt. *Gondwana Research*, **21:**451-465.

Banner J.L. & Hanson G.N. 1990. Calculation of simultaneous isotopic and trace element variations during water-rock interaction with application to carbonate diagenesis. *Geochimica et Cosmochimica Acta*, **54:**3123-3137.

Basu A.R., Jacobsen S.B., Poreda R.J., Dowling C.B. and Aggarwal P.K. 2001. Large groundwater strontium flux to the oceans from the Bengal Basin and the marine strontium isotope record. *Science*, **293:**1470-1473.

Beck A.J., Charette M.A., Cochran J.K., Gonneea M. E., Peucker-Ehrenbrink B. 2013. Dissolved strontium in the subterranean estuary – Implications for the marine strontium isotope budget. *Geochimica et Cosmochimica Acta*, **117:**33-52.

Brand U. & Veizer J. 1980. Chemical diagenesis of a multicomponent carbonate system-1: Trace elements. *Journal of Sedimentary Petrology*, **50:**1219-1236.

Brass G.W. 1976. The variation of the marine $^{87}Sr/^{86}Sr$ ratio during Phanerozonic time: interpretation using a flux model. *Geochimica et Cosmochimica Acta*, **40:**721-730.

Buchwaldt R., Toulkeridis T., Babinski M., Santos R., Noce C.M., Martins-Neto M.A., Hercos C.M. 1999. Age determination and age-related provenance analysis of the Proterozoic glaciation event in central-eastern Brazil. In: SSAGI, South American Symposium on Isotope Geology, Cordoba, Argentina, *Actas*, p. 387-390.

Caxito F.A., Halverson G.P., Uhlein A., Stevensson R., Dias T.G., Uhlein G.J. 2012. Marinoan glaciation in east Central Brazil. *Precambrian Research*, **200-203:**38-58.

Chemale F., Alkmim F.F., Endo I. 1993. Late Proterozoic tectonism in the interior of the São Francisco craton. In: Findlay, R.H., *et al.* (Eds.), *Gondwana Eight-Assembly, Evolution and Dispersal*. Balkema, pp. 29-42.

Claypool G.E., Kaplan I.R. 1974. The origin and distribution of methane in marine sediments. In: Kaplan I.R. (Ed.), *Natural Gases in Marine Sediments*. Plenum, New York, pp. 99-139.

Coelho J.C.C., Martins-Neto M.A., Marinho M. 2008. Estilos estruturais e evolução tectônica da porção mineira da bacia proterozoica do São Francisco. *Revista Brasileira de Geociências*, **38:**149-165.

Costa M.T. & Branco J.R. 1961. Roteiro para a excursão Belo Horizonte-Brasília. In Congresso Brasileiro de Geologia 14, UFMG, Belo Horizonte. *Instituto de Pesquisas Radioativas*, 15, 25p.

Dardenne M.A. 1978. Síntese sobre a estratigrafia do Grupo Bambuí no Brasil Central. In: Congresso Brasileiro de Geologia, 30, Recife, *Anais, SBG*, v. 2, p. 597-610.

Derry L.A., Kaufman A.J., Jacobsen S.B. 1992. Sedimentary cycling and environmental changes in the Late Proterozoic: Evidence from stable and radiogenic isotopes. *Geochimica et Cosmochimica Acta*, **56:**1317-1329.

Derry L.A. 2010. A burial diagenesis origin for the Ediacaran Shuram-Wonoka carbon isotope anomaly. *Earth and Planetary Science Letters*, **294:**152-162.

Dowling C.B., Poreda R.J., Basu A.R. 2003 The groundwater geochemistry of the Bengal Basin: Weathering, chemsorption, and trace metal flux to the oceans. *Geochimica et Cosmochimica Acta*, **67**(12):2117-2136.

Eyles N. & Januszczak N. 2004. `Zipper-rift´: a tectonic model for Neoproterozoic glaciations during the breakup of Rodinia after 750 Ma. *Earth-Science Reviews*, **65:**1-73.

Fölling P.G. & Frimmel H.E. 2002. Chemostratigraphic correlation of carbonate successions in the Gariep and Saldania Belts, Namibia and South Africa. *Basin Research*, **14:**69-88.

Frimmel H.E. 2010. On the reliability of stable carbon isotopes for Neoproterozoic chemostratigraphic correlation. *Precambrian Research*, **182**(4):239-253.

Grotzinger J.P., Waters W.A., Knoll A.H. 2000. Calcified metazoans in thrombolite–stromatolite reefs of the terminal Proterozoic Nama Group, Namibia. *Paleobiology*, **26**(3):334-359.

Guacaneme C., Babinski M., Paula-Santos G.M, Kuchenbecker M., Pedrosa-Soares A.C. 2014. Carbon and oxygen isotope stratigraphy of a section of the Sete Lagoas Formation (Bambuí Group) in southern São Francisco Craton, Brazil. In: SSAGI, South American Symposium on Isotope Geology, 9, São Paulo, Brazil. *Program & Abstracts*, p. 200.

Guacaneme C. 2015. *Geoquímica isotópica e elementar dos carbonatos da Formação Sete Lagoas, Grupo Bambuí, no sul da bacia do São Francisco*. MS Dissertation, Instituto de Geociências, Universidade de São Paulo, 131 p.

Halverson G.P., Hoffman P.F., Schrag D.P., Maloof A.C., Rice A.H. 2005. Toward a Neoproterozoic composite carbon-isotope record. *GSA Bulletin*, 117: 1181-1207.

Halverson G.P., Dudás F.O., Maloof A.C., Bowring S.A. 2007. Evolution of the $^{87}SR/^{86}SR$ composition of Neoproterozoic seawater. *Palaeogeography, Palaeoclimatology, Palaeoecology*, **256**(3-4):103-129.

Halverson G.P., Wade B.P., Hurtgen M.T., Barovich K.M. 2010. Neoproterozoic chemostratigraphy. *Precambrian Research*, 182:337-350.

Hebert C.L., Kaufman A.J., Penniston-Dorland S.C., Martin A.J. 2010. Radiometric and stratigraphic constraints on terminal Ediacaran (post-Gaskiers) glaciations and metazoan evolution. *Precambrian Research***, 182:**402-412.

Hoffman P.F., Kaufman A.J., Halverson G.P., Schrag D.P. 1998. A Neoproterozoic Snowball Earth. *Science*, **281:**1342-1346.

Hoffman P.F. & Schrag D.P., 2002. The Snowball Earth hypothesis: testing the limits of global change. *Terra Nova*, **14:**129-155.

Hoffman P.F. & Li Z.X. 2009. A palaeogeographic context for Neoproterozoic glaciation. *Palaeogeography, Palaeoclimatololy, Palaeoecology*. **277:**158-172.

Iglesias M. & Uhlein A., 2009. Estratigrafia do Grupo Bambuí e coberturas fanerozoicas no vale do rio São Francisco, norte de Minas Gerais. *Revista Brasileira de Geociências*, **39**(2):256-266.

Iyer S.S., Babinski M., Krouse H.L., Chemale F. 1995. Highly ^{13}C enriched carbonate and organic matter in the Neoproterozoic sediments of the Bambuí Group, Brazil. *Precambrian Research*, **73:**271-282.

Jacobsen S.B. & Kaufman A.J. 1999. The Sr, C and O isotopic evolution of Neoproterozoic seawater. *Chemical Geology*, **161:**37-57.

Kasemann S.A., von Strandmann P.A.E.P., Prave A.R., Fallick A.E., Elliot T., Hoffmann K.H. 2014. Continental weathering following a Cryogenian glaciation: Evidence from calcium and magnesium isotopes. *Earth and Planetary Science Letters*, **396:**66-77.

Kaufman, A.J., Jacobsen, S.B. and Knoll, A.H., 1993. The Vendian record of Sr and C isotopic variations in seawater: Implications for tectonics and paleoclimate. *Earth Planetary Science Letters*, **120:**409-430.

Kaufman, A.J., Knoll, A.H., Narbonne, G.M., 1997. Isotopes, ice ages, and terminal Proterozoic Earth history. *National Academy Sciences Proceedings*, **94:**600-605.

Kaufman A.J., Sial A.N., Frimmel H.E., Misi A., 2009. Neoproterozoic to Cambrian palaeoclimatic events in southwestern Gondwana. In: Gaucher C., Sial A.N., Halverson, G.P, Frimmel H.E. (Eds.): Neoproterozoic-Cambrian Tectonics, Global Change and Evolution: a focus on southwestern Gondwana. Developments in Precambrian Geology, 16, Elsevier, pp. 369-388.

Kennedy M.J. 1996. Stratigraphy, sedimentology and isotope geochemistry of Australian Neoproterozoic glacial cap dolostones: deglaciation, δ¹³C excursions and carbonate precipitation. *Journal of Sedimentary Research*, **66:**1050-1064.

Kirschvink J.L. 1992. Late Proterozoic low latitude glaciations: the snowball Earth. In: Schopf J.W. & Klein C. (eds.), *The Proterozoic Biosphere: A Multidisciplinary Study*. Cambridge, Cambridge University Press, p. 51-52.

Knoll A.H., Hayes J.M., Kaufman A.J., Swett K., Lambert I.B. 1986. Secular variation in carbon isotope ratios from upper Proterozoic successions of Svalbard and East Greenland. *Nature*, **321:**832-837.

Kuchenbecker M. 2011. *Quimioestratigrafia e proveniência sedimentar da porção basal do Grupo Bambuí em Arcos (MG)*. MS Dissertation, Instituto de Geociências, Universidade Federal de Minas Gerais, Belo Horizonte, 91 p.

Kuznetsov A.B., Gorokhov I.M., Semikhatov M.A., Melnikov N.N., Kozlov V.I. 1997. Strontium isotopic composition from the Inzer Formation limestones, the Upper Riphean type section in southern Urals. *Trans. Russian Acad. Sci., Earth Sci. Sections*, 353:319-324.

Kuznetsov A.B., Ovchinnikova G.V., Gorokhov I.M., Letnikova E.F., Kaurova O.K., Konstantinova G.V. 2013. Age constraints on the Neoproterozoic Baikal Group from combined Sr isotopes and Pb-Pb dating of carbonates from the Baikal type section, southeastern Siberia. *Journal of Asian Earth Sciences*, **62:**51-66.

Martins-Neto M.A., Pedrosa-Soares A.C., Lima S.A.A. 2001. Tectono-sedimentary evolution of sedimentary basin from Late Paleoproterozoic to Late Neoproterozoic in the São Francisco craton and Araçuaí fold belt, eastern Brazil. *Sedimentary Geology*, **142:**343-370.

Martins-Neto M.A. 2005. A Bacia do São Francisco: arcabouços estratigráfico e estrutural com base na integração de dados de superfície e subsuperfície. III Simpósio sobre o Cráton do São Francisco, Salvador/BA, 2005, *Anais*, p. 283-286.

Martins-Neto M.A. 2009. Sequence stratigraphic framework of Proterozoic successions in eastern Brazil. *Marine and Petroleum Geology*, **26:**163-176.

Melezhik V.A., Gorokhov, I.M., Kuznetsov, A.B., Fallick, A.E., 2001. Chemostratigraphy of Neoproterozoic carbonates: implications for "blind dating". *Terra Nova*, **13:**1-11.

Melezhik V.A., Pokrovsky B.G., Fallick A.E., Kuznetsov A.B., Bujakaite M.I. 2009. Constrain on ⁸⁷Sr/⁸⁶Sr of Late Ediacaran seawater: insight from high-Sr Siberian limestones. *Journal of the Geological Society*, **166:**183-191.

Misi A. & Veizer J. 1998. Neoproterozoic carbonate sequences of the Una Group, Irece Basin, Brasil: chemostratigraphy, age and correlations. *Precambrian Research*, **89:**87-100.

Misi A., Kaufman A.J., Veizer J., Powis, K., Azmy, K., Boggiani, P.C., Gaucher, C., Teixeira J.B.G., Sanchez, A.L., Iyer, S.S.S., 2007. Chemostratigraphic correlation of Neoproterozoic successions in South America. *Chemical Geology*, 237:143-167.

Moore W.S. 2010. The effect of submarine groundwater discharge on the ocean. *Annual Review of Marine Science*, **2:**5-88.

Narbonne G. 2008. The Gaskiers glaciation as a significant divide in Ediacaran history and stratigraphy. *Abstracts*, International Geological Congress.

Paula-Santos G.M., Babinski M., Kuchenbecker M., Caetano-Filho S., Trindade R.I., Pedrosa-Soares A.C. 2015. New evidence of an Ediacaran age for the Bambuí Group in southern São Francisco craton (eastern Brazil) from zircon U-Pb data and isotope chemostratigraphy. *Gondwana Research*, **28**(2):702-720.

Pedrosa-Soares A.C., Campos C.P., Noce C., Silva L.C., Novo T., Roncato J., Medeiros S., Castañeda C., Queiroga G., Dantas E., Dussin I., Alkmim F.F. 2011. Late Neoproterozoic-Cambrian granitic magmatism in the Araçuaí orogen (Brazil), the Eastern Brazilian Pegmatite Province and related mineral resources. *Geological Society of London Special Publications*, **350:**25-51.

Palmer M.R. & Edmond J.M. 1989. The strontium isotope budget of the modern ocean. *Earth and Planetary Science Letters*, **92:**11-26.

Pierre, C., 1989. Sedimentation and diagenesis in restricted marine basins. *In*: Fritz, P., Fontes, J.C.H. (Eds.) *Handbook of Environmental Isotope Geochemistry*, v.3 The Marine Environment. A. Elsevier, Amsterdam, p. 257-315.

Pimentel M.M., Fuck R.A., Botelho N.F. 1999. Granites and the geodynamic history of the Neoproterozoic Brasilia belt, Central Brazil: A review. *Lithos*, **46**(3):463-483.

Rahaman W. & Singh S.K. 2012 Sr and ⁸⁷Sr/⁸⁶Sr in estuaries of western India: Impact of submarine groundwater discharge. *Geochimica et Cosmochimica Acta*, **85:**275-288.

Ribeiro J.H., Tuller M.P., Danderfer A. 2003. *Mapeamento Geológico região Sete Lagoas, Pedro Leopoldo, Matozinhos, Lagoa Santa, Vespasiano, Capim Branco, Prudente de Morais, Confins e Funilândia. Estado de Minas Gerais. Escala 1:50000* Texto explicativo PROJETO VIDA, Serviço Geológico do Brasil.

Rocha-Campos A.C. & Hasui Y. 1981. Tillites of the Macaúbas Group (Proterozoic) in central Minas Gerais and southern Bahia, Brazil. *In*: Hambrey, M. J., Harland, W. B. (Eds) *Earth's pre-Pleistocene Glacial Record*. Cambridge University Press, p. 933-939.

Rodrigues J.B. 2008. *Proveniência de sedimentos dos grupos Canastra, Ibiá, Vazante e Bambuí* – um estudo de zircões detríticos e idades modelo Sm-Nd. PhD. Thesis, Instituto de Geociências, Universidade de Brasília, Brasília, 128 p.

Santos R.V., Alvarenga C.J.S., Dardenne M.A., Sial A.N., Ferreira V.P. 2000. Carbon and oxygen isotope profiles across Meso-Neoproterozoic limestones from central Brazil: Bambuí and Paranoá Groups. *Precambrian Research*, **104:**107-122.

Santos R.V., Alvarenga C.J.S., Babinski M., Ramos M.L.S., Cukrov N., Fonseca M.A., Sial A.N., Dardenne M.A., Noce C.M., 2004. Carbon isotopes of Mesoproterozoic–Neoproterozoic sequences from Southern São Francisco craton and Araçuaí Belt, Brazil: Paleogeographic implications. *Journal of South American Earth Sciences*, **18:**27-39.

Schöll W.U. 1976. Sedimentologia e geoquímica do Grupo Bambuí na parte sudeste da Bacia do São Francisco. In Congresso Brasileiro de Geologia, 29, Ouro Preto, *Anais*, p. 207-231.

Schrag D., Higgins J., Macdonald F., Johnston D. 2013. Authigenic carbonate and the history of the global carbon cycle. *Science*, **339:**540.

Schrag D., Higgins J., Macdonald F., Johnston D., 2014. Authigenic carbonate and the history of the global carbon cycle: Why diagenesis matters even more. *Goldschmidt Abstracts*, **2223**.

Semikhatov, M.A., Gorokhov, I.M., Kuznetsov, A.B. et al., 1998. The strontium isotopic composition in early Late Riphean seawater: Limestones of the Lakhanda Group, the Uchur-Maya region, Siberia. Trans. (Dokl.) *Russian Academy of Sciences. Earth science sections*, **360:**488-492.

Shields G.A. 2007. A normalised seawater strontium isotope curve: possible implications for Neoproterozoic–Cambrian weathering rates and the further oxygenation of the Earth. *eEarth*, **2:**35-42.

Silva-Tamayo J.C., Nägler T.F., Villa I.M., Kyser K., Vieira L.C., Sial A.N., Narbonne G.M., James N.P. 2010. Global Ca isotope variations in c. 0.7 Ga old post-glacial carbonate successions. *Terra Nova*, 22:188-194.

Teixeira W., Sabaté P., Barbosa J., Noce C.M., Carneiro M.A. 2000. Archean and Paleoproterozoic tectonic evolution of the São Francisco craton, Brazil. In: Cordani U.G., Milani E.J., Thomaz-Filho A., Campos D.A. (eds.) *Tectonic Evolution of South America.* 31st International Geology Congress, Rio de Janeiro, p. 101-137.

Tuller M.P., Ribeiro J.H., Signorelli N., Feboli W.L., Pinho J.M.M. 2009. *Projeto Sete Lagoas-Abaeté, Estado de Minas Gerais: texto explicativo,* Belo Horizonte: CPRM.

Uhlein G.J., Uhlein A., Halverson G.P., Stevenson R., Caxito F.A., Cox G.M., Carvalho J.F.M.G. 2016. The Carrancas Formation, Bambuí Group: A record of pre-Marinoan sedimentation on the southern São Francisco craton, Brazil. *Journal of South American Earth Sciences,* **71:**1-16.

Vieira L.C., Almeida R.P., Trindade R.I.F., Nogueira A.C.R., Janikian L. 2007a. Formação Sete Lagoas em sua área-tipo: fácies, estratigrafia e sistemas deposicionais. *Revista Brasileira de Geociências,* **37:**1-14.

Vieira L.C., Trindade R.I.F, Nogueira A.C.R., Ader M. 2007b. Identification of a Sturtian cap carbonate in the Neoproterozoic Sete Lagoas carbonate plataform, Bambuí Group, Brazil. *Comptes Rendus Geoscience,* 339:240-258.

Warren L.V., Quaglio F., Riccomini C., Simões M.G., Poiré D.G., Strikis N.M., Anelli L.E. Strikis P.C. 2014. The puzzle assembled: Ediacaran guide fossil Cloudina reveals an old proto-Gondwana seaway. *Geology,* **42**(5):391-394.

Whithicar M.J., Faber E., Schoell M. 1986. Biogenic methane formation in marine and freshwater environments: CO_2 reduction versus acetate fermentation? Isotope evidence. *Geochimica et Cosmochimica Acta,* **50:**693-709.